Decoration of *nano*-Spikes on Polymeric Surfaces with Quaternized *N*- Chloramines for Enhanced Antibacterial Activity

By

Mahamuda Sultana

A Thesis Submitted to the Faculty of Graduate Studies of

The University of Manitoba in partial fulfillment of the requirement of

the degree of

Master of Science

Biosystems Engineering

University of Manitoba, Winnipeg, Canada

Copyright © 2024 by Mahamuda Sultana

Abstract

Contact active antibacterial surfaces have wide acceptance to prevent bacteria-related infection. Contact active antibacterial surfaces by the physical killing method are mostly used as implants in the human body and contact active antibacterial surfaces by the chemical killing method are extensively used in devices in hospital areas, the food industry, high touch surfaces, etc. In this study, we have engineered a novel polymeric surface that combines chemical and physical antibacterial strategies. This is achieved by integrating chemical-killing contact active biocides, specifically azido quaternized *N*-chloramine, with a physical killing approach inspired by the natural antibacterial properties of insect wings. Our fabrication process successfully replicates the *nano*-scale features of these natural surfaces on a polymer, incorporating *nano* spikes that are functionalized with an alkynyl handle. This handle facilitates a click chemistry reaction with the antibacterial agent *N*-chloramine.

The efficacy of the resulting surfaces, denoted as P_{nCl}, was evaluated against *Escherichia coli (E. coli*) and *Methicillin-resistant Staphylococcus aureus* (MRSA). Compared to the control surfaces P_n and P_{Cl}, P_{nCl} demonstrated superior antibacterial activity. Notably, it achieved a 100% reduction in *E. coli* populations within 15 minutes of contact and a complete eradication of MRSA within 60 minutes. This study underscores the potential of combining chemical and physical antibacterial strategies on a single surface, offering a promising avenue for developing advanced antimicrobial materials.

Acknowledgment

Firstly, I am grateful to almighty God for giving me the strength that helped me to pursue my graduate degree staying thousands of miles away from home and overcoming all obstacles in my personal life that I had to endure during this journey.

I would like to thank my advisor, Dr. Song Liu for his continuous support and guidance throughout the entire duration of my master's program at UofM. He has been a great mentor and guardian. I would doubt whether I could have come this far without his support from the first day of our meeting in his office and the perseverance he showed to me in all my graduate years. Doing research under his guidance was hard initially for me, but I express my gratitude to Dr. Liu for providing me with direction at every step and making it a joyful memorable academic journey. I would also like to thank him for the financial support he provided me during my master's program at UofM.

I would like to thank my committee members, Dr. Mashiur Rahman, and Dr. Chengbo Yang for their precious time despite their busy schedules.

I also want to thank my fellow lab mates Farinaz Jonidi Shariatzadeh, Sarah Currie, Quintin Litke, and Changning Yu in the Biomaterial Synthesis and Surface Engineering Lab for being kind and helpful. Working in the lab would not have been a pleasure without your presence. I have learned a lot from each of you and it is my pleasure to work with you all.

Finally, I would like to acknowledge the love and support of my beloved husband Adnan Alam Khan and dedicate this thesis to him.

Table of Contents

Abstract i

Acknowledgment ii

Table of Contents iii

List of Figures vi

List of Tables viii

Lists of Abbreviation ix

Chapter 1: Introduction 1

1.1 Present state of the problem and current remedy 1

1.1.1 Studies on artificially fabricated antibacterial surface 1

1.1.2 Studies on naturally occurring antibacterial surface: 2

1.2 Contact killing surface through the chemical method: Contact active biocide: 4

1.2.1 Contact active *N*-chloramine – modes of action: 4

1.2.2 Contact active QACs – modes of action: 6

1.3 Contact killing surface through physical method: (fabrication of spikes with patterns) 7

1.3.1 Fabrication of contact killing surface (physical method) by biomimicking natural biocidal surface 8

1.3.2 Cicada (*Cryptotympana aquila)* wing as natural *nano*-patterned antibacterial surface 8

1.3.3 The modes of action 10

1.4 Conventional techniques for artificial antibacterial surfaces by biomimicking natural antibacterial surfaces 11

1.5 UV cross-linkable polymerization 13

1.6 Click chemistry - A facile reaction to quipped *nano* pillar with antibacterial agent 13

1.7 Challenges in contact active antibacterial surfaces 15

Chapter 2: The Hypothesis and Objectives 17

Chapter 3: Materials and Methods 19

3.1 Materials 19

3.2 Cleaning procedure for cicada wings: 20

3.3 Preparation of polymer solution and transferring technique of cicada wings pattern to prepare negative mold 20

3.4 Preparation of MBAA functionalized polymer solution and fabrication of positive pattern (cicada wing's pattern) mold from negative patterned mold 21

3.5 Click linkage between antibacterial agent and MBAA functionalized *nano* pillars 23

3.6 Chlorination of PEGDA *nano* patterned surface with *N*-Cl coating and PEGDA smooth surface with *N*-Cl coating and chlorine loading measurement 23

3.7 Instrumental analysis and characterization 24

3.8 Positive charge density measurements 25

3.9 Water contact angle measurement 26

3.10 Imaging of dead bacteria on nanopatterned PEGDA surface with *N*-Cl coating 26

3.11 Antibacterial assessment in phosphate buffered saline (PBS) 27

3.12 Statistical analysis 28

Chapter 4: Result and Discussion 29

4.1 Functionalization of PEGDA positive surface with MBAA 30

4.2 The topographical analysis of the *Cryptotympana aquila's* wing feature 31

4.3 Topographical analysis to analyze the fabricated negative patterned mold and MBAA functionalized PEGDA positive patterned mold 33

4.4 ATR-FTIR spectra for MBAA functionalized PEGDA after click reaction 38

4.5 Chlorination and chlorine loading study 39

4.6 Elemental mapping analysis to confirm active chlorine on the P_{nCl} surface 40

4.7 Positive charge density measurement: 42

4.8 Water contact angle measurements: 42

4.9 Assessment of antibacterial activity in PBS solution 44

4.10 SEM micrographs of bacteria on the chlorinated P_{ncl} surface 48

Chapter 5: Conclusions 49

Chapter 6: Future Work 51

References 53

List of Figures

Figure 1. Schematic showing bacteria-nano-structured surface interaction of a, b cicada wing and gram-negative bacteria, c, d cicada wing and gram-positive bacteria, e–g dragonfly wing and gram-negative bacteria, h, i dragonfly wing and gram-positive bacteria, j, k gecko skin and gram-negative bacteria and i gecko skin and gram-positive bacteria. Nano-structure dimensions are indicated next to each species, dimensions not to scale [47]. (Copyright © 2017)..... 10

Figure 2. Cu(I)-catalyzed alkyne-azide cycloaddition..... 14

Figure 3. The dead Cicada (Cryptotympana quila) 19

Figure 4. Preparation of PPGDA negative mold from cicada wing's..... 21

Figure 5. Preparation of MBAA functionalized PEGDA mold from PPGDA negative mold 22

Figure 6. ATR-FTIR spectra of a) PEGDA film and b) polyMBAA functionalized PEGDA film..... 31

Figure 7. SEM images of Cryptotympana aqulia's wing with three different magnifications (20,000×,100,000× and 150,000×)..... 32

Figure 8. SEM images of Cryptotympana aqulia's wing's cross-sectional view with two different magnifications..... 32

Figure 9. Frequency distribution of *nano*-pillars(n=100) height(nm) and tip diameter(nm) of Cryptotympana aquila's wings..... 33

Figure 10. SEM images of negative mold prepared from PPGDA with two different magnifications (50,000× and 120,000×) 34

Figure 11. Frequency distribution of *nano*-pillars (n=100) basal diameter(nm) and tips diameter(nm) of negative mold prepared from PPGDA..... 34

Figure 12. SEM images of Positive Patterned mold prepared from polyMBAA functionalized PEGDA with three different magnifications (25,000×,50,000× and 80,000×) 35

Figure 13. SEM images of Positive Patterned mold prepared from polyMBAA functionalized PEGDA's cross sectional view with two different magnifications. 36

Figure 14. Frequency distribution of *nano*-pillars(n=100) height(nm) and tip diameter(nm) of poly MBAA functionalized PEGDA 36

Figure 15. ATR-FTIR spectra of a) polyMBAA functionalized PEGDA film and b) polyMBAA functionalized PEGDA film after click reaction with C1. 38

Figure 16. EDX analysis of PEGDA nano-patterned surface with C1 Elemental mapping Image analysis of PEGDA nano-patterned surface with C1 a) Morphology of fabricated film b) Energy dispersive X-ray spectroscopy of C) carbon d) Oxygen e) Chlorine f) homogeneous distribution of C, O and Cl on the P_{nCl} surface. 40

Figure 17. EDX analysis of PEGDA nano-patterned surface with C1: Spot 1 the surface area and Spot 2 the cross section of the sample. 41

Figure 18. images of a 2 µL droplet of water on the a) wing b) wings pattern on the PEGDA surface c) PEGDA smooth surface, PEGDA with *N*-Cl coating, and PEGDA with *N*-Cl coating with the pattern as seen with the WCA instrumentation and water contact angle of all surfaces (table in upper left corner) 43

Figure 19. Log Reduction P_n, P_{Cl}, and P_{nCl} compared to Control at 3 different time points for *E. coli* and MRSA (different alphabet indicates significant difference within each group and P-value < 0.01). 47

Figure 20. Cell damages caused by PEGDA with *N*-Cl coating with pattern (P_{nCl}) *E. coli* (L) and MRSA (R) 48

Lists of Tables

Table 1 Dimension of (height and tips and basal diameter) Master substrate, negative mold and positive mold..... 37

Table 2 Active chlorine loading on the smooth surface with *N*-Cl coating and nano-patterned surface with an *N*-Cl precursor structure after the first time of chlorination. 39

Table 3 Percentage of active chlorine on PEGDA *nano*-patterned surface with C1..... 41

Table 4 Positive Charge Density Measurement of PEGDA smooth surface and PEGDA *nano* Patterned surface after chlorination 42

Table 5 Antibacterial efficacy of a) PEGDA smooth surface b) wings pattern on PEGDA surface c) PEGDA smooth surface with *N*-Cl coating, and PEGDA with *N*-Cl coating with the pattern against *E. coli.* 46

Table 6 Antibacterial efficacy of a) PEGDA smooth surface b) wings pattern on PEGDA surface c) PEGDA smooth surface with *N*-Cl coating, and PEGDA with *N*-Cl coating with the pattern against *MRSA* 47

Lists of abbreviation

MBAA: N-(2-methylbut-3-yn-2-yl) acrylamide

PEGDA: Polyethylene glycol diacrylate

PPGDA: Polypropylene glycol diacrylate

QACs: Quaternary ammonium compounds

N-Cl: *N*-Chloramine

PI: Photo initiator

CuAAC: Cu(I)-catalyzed alkyne-azide cycloaddition

WCA: Water contact angle

UV: Ultra violate

MRSA: Methicillin-resistant *Staphylococcus aureus*

E. Coli: *Escherichia coli*

PBS: Phosphate-buffered saline

Chapter 1: Introduction

1.1 Present state of the problem and current remedy

The proliferation and buildup of bacteria on surfaces are widely observed phenomena across diverse fields, including food packaging, pharmaceuticals, biomedical devices, and implants. This bacterial growth not only results in significant property damage but also poses substantial health risks, highlighting its profound consequences. [1]. Further, in recent years, infections caused by bacteria resistant to antibacterial agents have become a major health concern. This resistance has made conventional bactericidal therapy less effective for many infectious diseases. Bacteria protect themselves from the bactericidal agents by forming a self-made polysaccharide matrix, usually known as biofilms. They attach to solid-air interfaces of healthcare units such as curtains, hospital trolleys, glass door [2]. The transmitting of vehicle-borne bacteria needs to be broken to prevent bacterial infection. The fabrication of contact active biocidal surface is an efficient approach to minimize bacterial infection in hospitals, the food industry, restaurants as microbial contamination occurring in those areas inevitably leads to biofilms formation, linked to numerous multi-resistant bacterial strains [3],[4].

1.1.1 Studies on artificially fabricated antibacterial surface

The immobilization of antibacterial moiety through a durable bond (mostly covalent bond) on the material surface is one of the promising approaches for fabricating contact active bactericidal surface [5].

Various biocides have been adopted to make inert material surface lethal against broad spectrum bacteria; for instance, commonly known contact active biocides, such as, Quaternary ammonium compounds (QACs), peptides, *N*-Chloramines are immobilized on surfaces with covalent bond that inactivate bacteria upon contact [6],[7],[8].

Among them, organic *N*-chloramines are the most employed antibacterial agents, and their bactericidal efficacy matches with chlorine bleach solution in a safer way [9]. A key advantage of *N*-chloramines is their ability to be recharged using chlorine bleach solution, and no bacterial resistance has yet been reported against *N*-Chloramines [10]. *N*-chloramine is a group of compounds containing one or more *N*-Cl single bonds and is oxidative enough to kill bacteria. Initially, the external protein matrix of bacteria undergoes chlorination, resulting in the formation of a moderate chlorine cover. Subsequently, oxidative chlorine infuses bacterial cells, targeting numerous vital components, including enzymes containing thiols and thioethers, through oxidation. Additionally, proteins are denatured through trans-chlorination. It's evident that these reactions lead to the eventual death of the bacteria and the transformation of *N*-chloramines into their precursor, N-Hs. [11], [12]. Upon chlorine bleaching of N-Hs, it regains its bacteria-killing capacity as the reverse reaction.

1.1.2 Studies on naturally occurring antibacterial surface:

Another promising approach for killing bacteria is a physical method using the contact killing mechanism, inspired by nature instead of chemical killing bacteria. Those antibacterial surfaces are fabricated by bio mimicking several insects, animals, and plants. The presence of nano/microstructures on their surfaces can kill bacteria physically rather than chemically [13].

Researchers also put their effort into generating artificial patterning with 3D microstructure with different shapes like conical, square, spikes, round, etc., to prevent biofilm formation for some bacteria. The presence of sharp pillar-like structures (micro/ *nano*) with various diameters, height, and pitch (ranging from micro to *nano* range) is responsible for the bactericidal effects of these surfaces, which pierce into the bacterial cell wall upon contact or rupturing the bacteria cell wall, thereby destroying its vital organ. Up to now, researchers have established two models to explain bacterial cell death due to the nanotextured surface: (1) a biophysical model [14] and (2) an analytical thermodynamic model.

The biophysical model regards the bacterial cell membrane as a thin, elastic layer. The majority of bacterial cells are within the micrometer scale, whereas bactericidal surfaces are typically within the nanometer range. This discrepancy in scale leads to the division of the adsorbed layer into two regions: one in direct contact with the pillar and another suspended between pillars. Cell rigidity of bacterial cell membranes is another key factor to be considered in the biophysical model. This factor better explains why *nano* pillar textured surface is bactericidal towards less rigid gram-negative bacteria compared to gram-positive bacteria [14].

Li introduced the analytical thermodynamic approach, which elucidated the bactericidal mechanism of *nano*-patterned surfaces by examining the overall free energy alteration of bacterial cells adhering to the patterned surface.

According to this model, the top of the *nano*-pillar ridges stretches the bacteria's outer membrane at the highest level [15]. The maximum membrane stretching capacity of gram-negative bacteria is higher than that of gram-positive bacteria because the gram-negative bacteria contain 1–3 layers of peptidoglycans (1–3 layers) and the gram-positive cells possess 10–50 layers [16], [17].

The artificial *nano* /micro pillar textured surface can be tuned so that multi-antibiotic-resistant bacteria can be treated effectively with this physical bactericidal method [18].

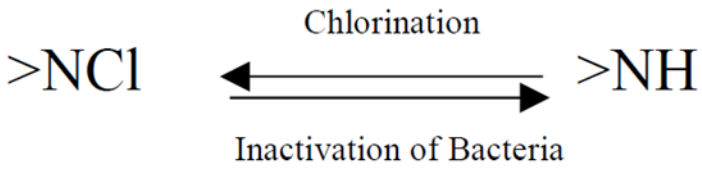
1.2 Contact killing surface through the chemical method: Contact active biocide:

Antibacterial agents that are contact-active can attach to the substrate only once and kill bacteria without producing any environmental hazard. These contact-active antibacterial agents are categorized as non-leaching type biocides as they emit zero pollution and transfer active agents to inactive bacteria. Further, surfaces with contact-active agents do not affect bacterial resistance; rather, they only result in real damage to the bacterial cell in a nonspecific way by exerting oxidative stress instead of targeting a particular objective such as mitochondria and ribosomes [19]. In general, contact-active biocidal surfaces are constructed by physically or chemically infusing contact-active antibacterial agent in surfaces (e.g., glass and metal) [20], [21]. In the below section, *N*-chloramine and QACs is discussed.

1.2.1 Contact active *N*-chloramine – modes of action:

N-chloramines refer to compounds containing one or more nitrogen-chlorine covalent bonds, typically formed through the chlorination of amine, amide, or imide. These compounds may be linked to either organic or inorganic groups [9]. The three types of organic *N*-chloramines are

Imide (-C(O)-NCl-C(O)-), amide (-C(O)-NCl-R) and amine (RR'-NCl). Followed by amide and amine, imides exhibit the lowest stability against hydrolysis. (imide < amide < amine), This instability against hydrolysis has a reverse effect on the antibacterial activity, and imide shows highest antibacterial activity, the highest to lowest antibacterial activity order is (imide > amide >> amine). For an immediate antimicrobial activity, imide *N*-chloramine compound is better suited and for a long-term activity, amine *N*-chloramine is the better choice.



Initially, free *N*-chloramines attack bacteria's outer protein matrix, by creating a moderate chlorine covering, cellular death is not necessarily ensured [22],[23],[24]. Subsequently, unbound *N*-chloramine permeates bacterial cells, oxidizing numerous crucial cellular components (including enzymes) containing thiol and thioethers, and inducing protein denaturation through transchlorination, ultimately leading to bacterial death [11]. As a biocide, *N*-chloramine acts on multiple targets nonspecifically. Therefore, it is less likely for bacteria to develop resistance against *N*-chloramine [25],[26]. *N*-chloramines may be reverted to the precursor chemicals after interaction with bacteria and formed again upon re-chlorination [27]. The distinct characteristic of *N*-halamine is rechargeability; after killing bacteria, *N*-chloramine loses its oxidative Cl^+. The transformation of the N-H group into *N*-Cl is a reversible process, allowing for the biocidal function on the surface to be recharged multiple times using chlorinating agents like chlorine bleach.

1.2.2 Contact active QACs – modes of action:

Quaternary ammonium compounds (QACs) feature positive nitrogen in their structure, connected to a covalent bond to four distinct groups[28]. Antibacterial effects of QACs result from the electrostatic interaction between the negatively charged bacteria and the positively charged QACs [28]. Electrostatic contact between the bacterial cell and the charged antibacterial drug can result in cell death through many indicated routes [11]. The QAC's ability to disrupt the cell membrane shows its antibacterial properties [29]. They have been introduced as antibacterial agents to different surfaces, and their activity mode of action on a surface is discussed in the following.

The end positive charge of a long spacer can infuse the bacteria cell, punching a hole in its peptidoglycan layer and indicating a polymeric spacer effect [11]. Certain studies have challenged the notion of the polymeric spacer effect as the mechanism behind QACs' antimicrobial activity, as altering the chain length of the antimicrobial agent did not impact its antimicrobial properties [30],[31],[32]. In 2005, according to Kugler et al. Proposal, an ion-exchange mechanism for bactericidal effect [33]. According to this mechanism of biocidal properties of QACs is the exchange of divalent cations on the bacteria with charged membrane, leading to killing of the bacteria cell. When the bacteria attach to the QACs on the surface, removal of Mg^{+2} and Ca^{2+} will be carried out in the case of *S. aureus* [33].

The phospholipid sponge effect is the newest proposed mechanism of QACs where the bacteria cell membrane contains the negatively charged phospholipids are attached to a oppositely charged surface [34]. This mechanism is confirmed by Asri et al., where they observed the

immobilization of QACs on a surface as the anionic-charged phospholipids on the side of the bacteria were removed, which was in contact with the surface [35].

The antimicrobial properties of QACs can be affected by several factors. Charge density is one of the important factors that have a threshold for the surface charge effectively combat bacteria. According to Kugler et al., the antibacterial action of a surface against *S. epidermidis* and *E. coli*, the threshold of 10^{14} charge/cm^2 must be met when the bacteria cell met the low division and 10^{12} charge/cm^2 when in the high division. They have also verified that the negative charge on *S. epidermidis* is approximately 10^{13} negative charges/cm^2. To eliminate *E. coli*, more than 5×10^{14} positive charges/cm^2 are necessary as demonstrated by Murata et al., where [36] it is also observed interestingly, that the surface negative charge density of *E. coli* is between 5×10^{14} and 5×10^{15}. Alkenyl chain length is also to be considered an important factor for the biocidal activities of various QACs compounds where the 14-carbon and 16-carbon structures of QACs have shown to be optimal figures for the deactivation of Gram-positive and Gram-negative bacteria respectively [37].

1.3 Contact killing surface through physical method: (fabrication of spikes with patterns)

The bottom-up approaches at the *nano/*micro level offer a unique surface topography for preventing bacterial attachment or inactivation of bacteria through cell-surface interaction. The attachment of bacteria and biofilm formation on a material surface depends on the influencing factor of electrostatic interactions, hydrophobicity and steric hindrance and van der Waals forces [38]. The “height, radius, and spacing’’ of *nano* and micro-structures with close pack geometry/ repeated patterns play a crucial role in measuring the bacteria-specific efficacy [39].

1.3.1 Fabrication of contact killing surface (physical method) by biomimicking natural biocidal surface

The inspiration for fabricating artificial *nano*-structured biocidal or anti-biofouling surfaces came from specific nano topographies of insect wings, animal skin, plant leaves, and other natural surfaces [40]. The inclusion of hierarchical nanostructures, like hairs, pillars, needles, and plates, conferred natural anti-wetting and anti-biofouling traits upon the surfaces [41]. Lotus leaves, taro leaves, and sharkskin represent anti-biofouling surfaces contain the existence of micro and *nano* superhydrophobic structures and surface patterns prevent bacterial adhesion and cell attachment by repelling them. In contrast, dragonflies, gecko skin and cicada wings inactivate bacteria. Cicadas caught the special attention of researchers due to its hexagonal arrays of *nano*pillars found on its wing, which can show enhanced biocidal activity by lysing bacterial cells. The research study of Ivanova et al. shows that *nano*pillars present in cicada wings can kill *P. aeruginosa* cells within short time (3 min) of contact [42]. This distinguishes bactericidal activity of cicada wings draws researchers' special attention for biomimicking their surface topography on the artificial substrate to battle bacterial infection.

1.3.2 Cicada (*Cryptotympana aquila)* wing as natural *nano*-patterned antibacterial surface

In recent years Researchers fabricated contact-active antibacterial surfaces, inspired by natural resources as natural surfaces provide continuous sources of biocidal surfaces. According to the antibacterial behavior, the surfaces are categorized as either antifouling or bactericidal. Cicada wings caught the special attention of researchers for the presence of superhydrophobic *nano*-patterned spikes on their wings. Usually, cicadas are very easy to find in nature as they live underground, in tall trees, and can tolerate high temperatures and humidity. The surfaces of

the cicada wing are made of protein, chitin, and wax, which allows it to adapt to different conditions. The very special feature of cicada wings is the presence of the *nano* ranges' spikes like conical shape pilar in hexagonal arrays, but the dimensions (height, spacing, and diameter) differ among species [43]. Sun et al. studied 15 different species of cicada wing heights of *nano*pillar ranges from 159-246 nm, the diameter of *nano*pillars ranges from 82–148 nm, and 44–177 nm pillar spacing [44].

Ivanova et al. were the first to examine the bacterial properties of cicada wings where the attachment of *P. aeruginosa* (ATCC 9027) was studied on a specific species of cicada (*Psaltoda claripennis*) wing consisting of hexagonal arrays of conical shape *nano* pillars [45]. This research group further studied to identify whether the bactericidal action is chemical, physical or hydrophobic. The wing surfaces were sputter-coated with 10 nm gold to change the surface chemistry of the wings while maintaining the surface topography of natural *nano*-spike. The antibacterial activity against *P. aeruginosa* (ATCC 9027) remains unaltered by this modification of surface and revealed that bactericidal action was physically killing rather than chemical killing action [45].

This finding is further supported by the research study conducted by Hasan et al. The antibacterial inactivation of cicada wings was studied with a wide spectrum of gram-negative and gram- positive bacteria. According to their results, *nano* features array of wings was capable of constant killing of Gram-negative bacteria (*Escherichia coli, P. aeruginosa, Branhamella catarrhalis, P. fluorescens*), while Gram-positive bacteria (*Planococcus maritimus, Bacillus subtilis, Staphylococcus aureus*) remained unaffected towards the *nano*-patterned spikes [46].

1.3.3 The modes of action

It is generally accepted that the topographical features present on natural antibacterial surfaces are responsible for bacterial cell death. It is seen from Figure 1, that the arrays of pillar-like structure on cicada wings have a significant impact on gram-negative bacteria by rupturing their cell membrane while the gram-positive bacteria remain unaffected due to their thicker cell wall [45]. The microbial cell death is well explained by (1) a biophysical model and (2) an analytical thermodynamic model, which is the most acceptable method developed by researchers [47].

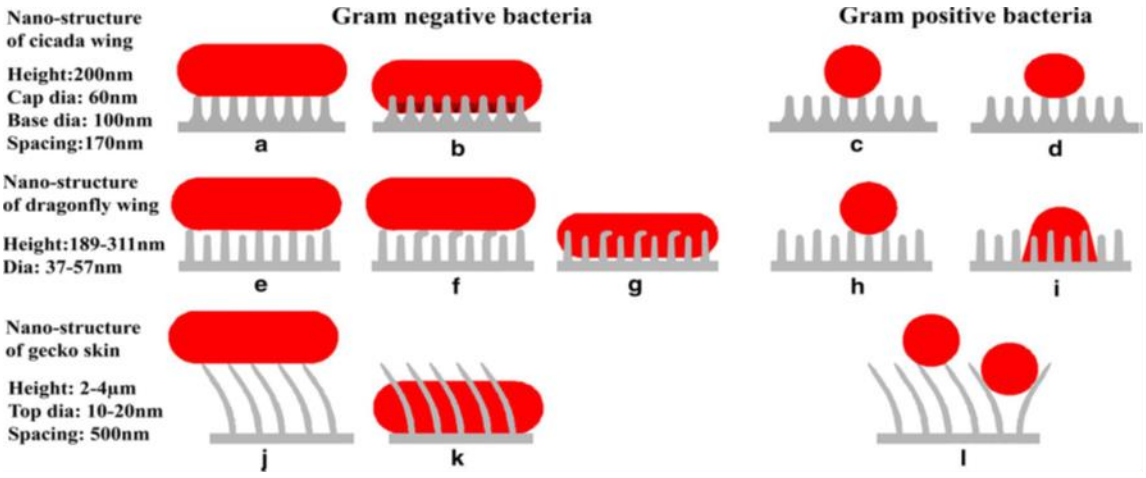


Figure 1. Schematic showing bacteria-nano-structured surface interaction of a, b cicada wing and gram-negative bacteria, c, d cicada wing and gram-positive bacteria, e–g dragonfly wing and gram-negative bacteria, h, i dragonfly wing and gram-positive bacteria, j, k gecko skin and gram-negative bacteria and i gecko skin and gram-positive bacteria. Nano-structure dimensions are indicated next to each species, dimensions not to scale [47]. (Copyright © 2017)

According to the biophysical model, bacteria retain their standard shape under a certain turgor pressure present because of a discrepancy of osmotic pressure between the inner and outer secondary shells. Further, the variance in thickness of peptidoglycan layers in bacteria's outer cells results in lower turgor pressure in Gram-negative cells than Gram-positive cells [48]. Contacting the bacterial cell wall with the nanopillars on *nano*structured surface results in a

massive pressure in bacteria's cell wall, increasing internal turgor pressure and cell wall thickness [14]. This increase in turgor pressure results in major stretching of cell membrane between nanopillars which causes rupturing of cell walls. Biophysical modelling of the above procedure on cicada wing surfaces for Gram-negative, rod-shaped bacteria indicates the procedure as an adsorption process of the nanopillar surface. When the bacterial cell contacts the *nano*pillar surface, the nanopillars absorb the bacterial membrane and hang a portion of the membrane between *nano*pillars [39].

In 2016, Li proposed an analytic thermodynamic model, according to this model, the microbial cell death is explained by the alteration of free energy of bacterial cell while attaching to the *nano*patterned surfaces [49]. According to this model, the individual free energy of bacterial cells is measured on flat surfaces and *nano*patterned surfaces. Then the changes in free energy are calculated by comparing these two surfaces, to get the stretching degree of outer cell bacteria. Due to the presence of *nano*pillar arrays on wings, the stretching degree of cell membrane increases enough to distress the outer membrane and caused eventual death of bacteria [49].

1.4 Conventional techniques for artificial antibacterial surfaces by biomimicking natural antibacterial surfaces

In the bioengineering field, a huge amount of research focused on the fabrication process of artificial antibacterial surfaces by biomimicking naturally occurring antibacterial surfaces. A combination of different chemical and physical methods involves replicating naturally occurring biocidal surfaces. The different types of lithography techniques for example electron beam

lithography, deep ultraviolet (UV) lithography, colloidal lithography, nano-imprint lithography (NIL) and X-ray lithography are the most widely used techniques for copying surface topography from the master substrate and then transferring it to the secondary substrate [49], [50]. Of these methods, colloidal lithography and nano-imprint lithography (NIL) are widely employed because of their high throughput and superior fabrication precision, especially for creating fine structures on the substrate's outer edges [51]. NIL involves the contact form of lithography where a natural antibacterial surface acts as a stamp, under conditions of elevated temperature and pressure, this stamp imprints on the resist substrate to transfer its geometrical *nano* features [47]. Micro molding technique provides faster fabrication of micro/*nano* features on polymer surfaces. The microstructural geometry of shark skin is transferred on epoxy resin using this method. The dimensional precision and degrees of reproducibility are comparatively higher in micro molding technique [51]. The vacuum casting method and the reactive ion etching method are used if the choice of substrate is silicon-based for artificial biocidal surface fabrication. In the reactive ion etching (RIE) method, plasma under vacuum conditions is generated due to the bombarding of high energy ions onto the silicon substrate to form the desired geometrical pattern of *nano*-structure [52]. Some research studies involve the biomimicking of dragonfly wing's nano-patterned structure onto black silica or silicon wafers [53]. The photolithography process is one of the most extensively used methods for fine-tuning of structural dimension of micro/*nano* patterned surfaces during the fabrication of artificial antibacterial surfaces. In this process, either negative or positive photoresist is spin-coated on the substrate surface, and then the desired pattern is transferred through a MASK after

exposure to UV light. The UV light changes the chemical structure of the photoresist. Soft baking, developing and hard baking process is involved to get the desired *nano* pattern [47].

1.5 UV cross-linkable polymerization

UV curing polymerization can be designed with tailored functionality by incorporating different monomers to make its surface functionalized along with varying their surface texture with different shapes. The UV curing method is well-established, fast, cost-effective, and requires simple equipment for its high throughput. In 2019, Kazemian et. al published their research work where they modified stainless steel (SS) to make it antibacterial by modifying the SS surface with silanization and then incorporating, N-(2-methylbut-3-yn-2-yl) acrylamide (MBAA) as the monomer through the crosslinker MBA using UV irradiation and benzophenone[52] In another study, Li et. al also functionalize poly (ethylene terephthalate) PET surfaces with (MBAA) as the monomer and *N,N'*-methylenebisacrylamide (MBA) as the crosslinker, Further reactions were done on the surface to make the surface antibacterial [53]. The UV-curable polymerization is highly preferable due to its zero requirement of high temperature and pressure. This additional quality makes it beneficial during the molding process when the natural sample surface is delicate and rare to find. Moreover, the surface texture of UV-curable materials could be finely tuned in terms of their physical aspects.

1.6 Click chemistry - A facile reaction to quipped *nano* pillar with antibacterial agent

Prior to the 21st century, Kolb and Sharpless; was the first research group who introduce the term "click Chemistry" as a novel and straightforward approach in the field of organic

chemistry. Click Chemistry represents a potent and versatile method where A pair of functional groups selectively connect under simple reaction conditions of an aqueous environment[54]. Kolb and Sharpless got his inspiration from nature to synthesize new potential drug molecules as the most complex chemical structure is formed in nature. The click chemistry is advantageous due to its high-yielding, simple, and 100% reaction conversion which means no by-product is formed and has greater use in bioscience[55]-[57], drug delivery[58], and material science[59]. Cu(I)-catalyzed alkyne-azide cycloaddition (CuAAC) is the most widely used click reaction. In this reaction, $CuSO_4$ is used along with sodium ascorbate (reducing agent). To maintain the aqueous environment mixtures of water with an acetone, Tetrahydrofuran (THF), alcohol, acetonitrile (MeCN), dioxane, dimethyl sulfoxide (DMSO), biphasic media mixing water with dichloromethane, and other mixtures of two or even three solvents are used for this reaction[60].

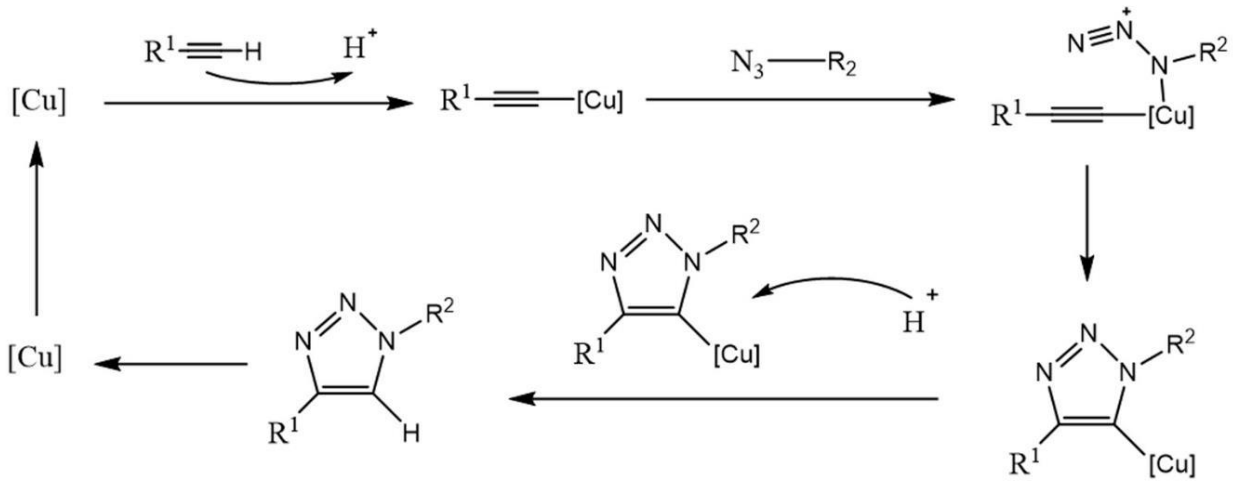


Figure 2. Cu(I)-catalyzed alkyne-azide cycloaddition

Nowadays researchers focus on click chemistry in surface modification by functionalizing polymers using click chemistry. In 2011, Li et. al. copolymerized PET surface with *N,N'*-methylenebisacrylamide (MBA, crosslinker), and monomer *N*-(2-methylbut-3-yn-2-

yl)acrylamide (MBAA) to functionalized PET surface with the alkynyl handle to be involved in "click" reactions with Azide [53]. In another work by Li et. al. a new biocide was introduced by modifying PET surface with cotton where Cu(I)-catalyzed alkyne-azide click reaction was utilized [61].

1.7 Challenges in contact active antibacterial surfaces

The conventional technique for biomimicking natural antibacterial surfaces onto an artificial surface has both pros and cons of above-mentioned techniques. The biggest obstacles are high fabrication costs associated with higher time consumption due to the complex steps involved in the fabrication procedure. The complex fabrication steps require expensive instruments to fabricate molding templates from natural antibacterial surfaces using the ion-based lithography method [62]. Though the Nanoimprint lithography (NIL) process is widely used, it also faces some limitations such as higher mold fabrication costs, damage of primary mold during separation from secondary mold, limited patterned size, also, removal of mold caused the damage to surface topography of secondary mold [63], [64]. In the micro molding method, it is possible to achieve similar dimensions of natural surfaces in terms of structure thickness, density, and spacing. In contrast, there are significant differences in terms of pillar height and tip diameter [65]. According to Zhang et al. study, significant changes in pattern height and tip diameter have been observed in the replication of shark skin topography. The high pressure attributed to the molding process is responsible for the bending and shrinkage of the pattern of shark skin preventing high-resolution replication [66].

Another important fact to consider is the clinical application of biomimetic *nano*-pillar array. The biomimetic natural antibacterial surface's antibacterial ability against Gram-positive bacteria is not as satisfactory as its antibacterial ability against Gram-negative bacteria [46]. Since both gram-negative and gram-positive bacteria are responsible for implant-associated infection, it is high time to focus on research to functionalize the *nano*pillar arrays with other antibacterial agents to make them effective against gram-positive strains to fulfill the bacteriostatic and bactericidal requirements of clinical application. In the recent work of Liu et al. group, they fabricated an antibacterial surface- cicada wing inspired Self-Adaptive *nano*composite Array by in situ assembly of bacteriostatic 3,3'-diaminodipropylamine (DADP)-doped zeolitic imidazolate framework-8 (ZIF-8), which shows significant efficacy against gram-positive bacteria [67] .

Chapter 2: The Hypothesis and Objectives

The focus of research has shifted towards developing new-generation antibacterial surfaces to reduce the occurrence of cross-contamination in HAIs. Our lab conducted a series of experiments to show that *N*-chloramines, quaternary ammonium (QA) compounds, and quaternized *N*-chloramines can be coated as effective contact active biocidal agents for engineering antibacterial surfaces. The "CuAAC" reaction provides click chemistry between *N*-chloramines moiety and alkynyl groups on various substrates like PET, stainless steel, textile, etc. On the other hand, a detailed investigation of various insect wings has exhibited that the *nano/* micro surface topography of wings influences bacterial cell death by physically rapturing bacterial cells. This feature implies that *nano*/ micro features possess the capability to address bacteria that have acquired resistance to chemical antibacterial interventions.

It is hypothesized that:

Enhanced antibacterial properties can be obtained by merging the chemical killing contact active method along with the physical killing approach by fabricating *nano-patterned* spike structure bonded with azido quaternized *N*-chloramine in a single surface.

In this study, a single polymeric surface is engineered as an effective antibacterial surface by combining chemical-killing contact active biocides with the physical killing approach by fabricating specific patterned *nano*/ bonded with azido quaternized *N*-chloramine.

The project aimed to achieve the goal by following the experimental steps given below:

1. Established a simple method for biomimicking natural antibacterial surfaces to fabricate *nano*-scale features on polymeric surfaces.
2. The fabricated cicada wings *nano* spikes feature was functionalized alkynyl handle to provide a click reaction site with antibacterial agent *N*-chloramine.
3. The presence of patterned *nano*-scale features on the polymeric surface increases the quantitative amount of active chlorine on the antibacterial agent *N*-chloramine by click reaction.
4. Based on any type of application, rapid bacteria kill is essential. Recent studies show that the fastest eradication of bacteria is crucial for the effective antibacterial performance of the coating, the goal of this project is to achieve boosted antimicrobial potency in terms of killing kinetics.

Chapter 3: Materials and Methods

3.1 Materials

Dead Cicadas (*Cryptotympana aquila)* mounted as wings spread were purchased from BioquipBugs. All solvents and chemicals such as acetone (99.0% anhydrous), 2-hydroxy-40-(2-hydroxyethoxy)-2-methylpropiophenone (98%) photo initiator (PI), polyethylene glycol diacrylate Mw 575 $gmol^{-1}$ (PEGDA), polypropylene glycol diacrylate Mw 800 $gmol^{-1}$ (PPGDA), Polyvinyl alcohol, sodium thiosulfate, copper(II) sulfate, Triton X-100, tert-butyl alcohol, dansyl azide, orange II dye, glutaraldehyde, and ascorbic acid sodium salt were purchased from Fisher and Sigma-Aldrich. Adhesive sealer tape was purchased from Home Depot which is used to create leakage-proof dikes around cicada wings and PPGDA negative patterned mold. Tryptone soya agar, Tryptone soya broth and Luria−Bertani (LB) broth were purchased from Thermo Scientific.

Alkynyl monomer *N*-(1,1-dimethylprop-2-ynyl) acrylamide (MBAA)[68] and *N*-(2-azidoethyl)-3-(4,4-dimethyl-2,5-dioxoimidazolidin-1-yl)-*N,N*-dimethylpropan-1-aminium (C1) were prepared according to the published procedures [69].



Figure 3. The dead Cicada (Cryptotympana quila)

3.2 Cleaning procedure for cicada wings:

The wings were gently detached from the cicada's body and cut into a small section (2.5 cm x 2 cm). Cicada wings were cleaned to remove dirt and the cleaning procedure involved 2 steps. First, sonicate in acetone for 10 minutes and then sonicate for 10 min in deionized water. Followed by dried under purified stream of air.

3.3 Preparation Of polymer solution and transferring technique of cicada wings pattern to prepare negative mold

Polymer precursor solution for negative mold was prepared by placing 30 mg 2-hydroxy-4'-(2-hydroxyethoxy)-2-methylpropiophenone (IRGACURE 2959) in a glass vial and dissolved in 0.5 mL of acetone, 3 mL of PPGDA at room temperature was added to this solution and vortexed for 90 second to ensure a homogenous solution [70] .

Figure 4. is the visual representation of preparing the negative pattern mold. The cleaned cicada wing is attached to the top of the glass slide with PVA glue, the edge of the wings should be secured with glue which will prevent the solution from traveling underneath the wings. The adhesive sealer tape is used to create a dike around the wing, the dike should be liquid-proof. 1.5 -2 mL of PPGDA solution is drop-cast inside the dike using a pipette.

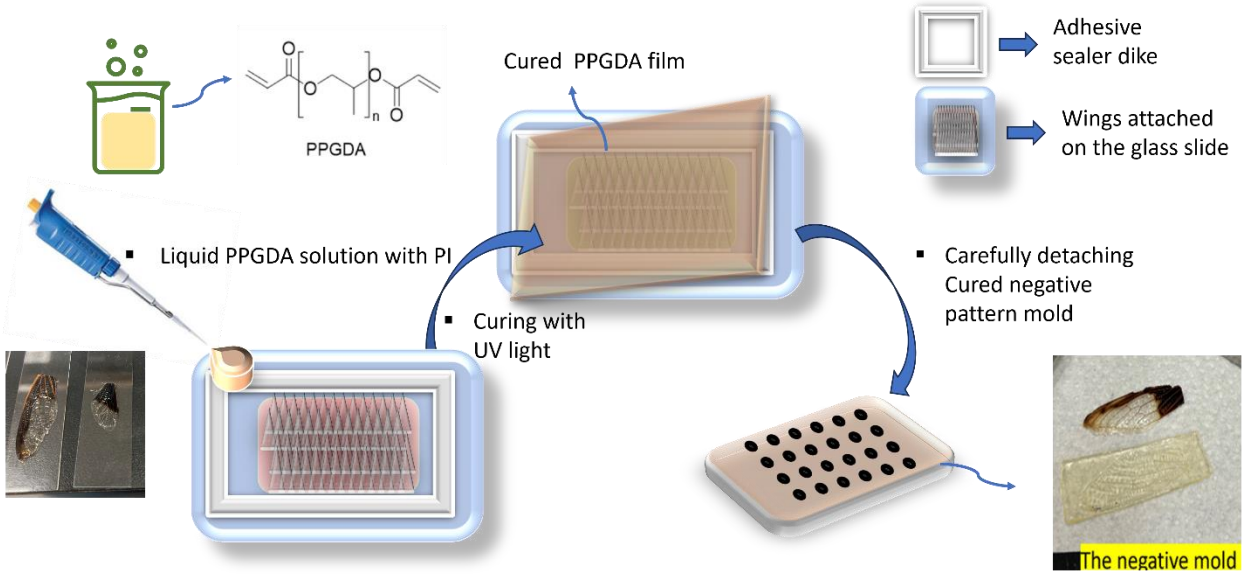


Figure 4. Preparation of PPGDA negative mold from cicada wing's

The curing of polymer solution to fabricate the negative patterned mold was carried out in the UV crosslinker: IntelliRay 400 at 365 nm wavelength with a 10 cm distance from the light source while maintaining 100% intensity. The exposure time for the PPGDA polymer solution was 2800 sec. After curing the negative patterned mold was carefully detached from the primary mold (wing) with a scalpel and tweezer.

3.4 Preparation of MBAA functionalized polymer solution and fabrication of positive pattern (cicada wing's pattern) mold from negative patterned mold

MBAA functionalized Polymer precursor solution for positive mold was prepared by placing 420 mg 2-hydroxy-4'-(2-hydroxyethoxy)-2-methylpropiophenone (PI) and 14.4 g of MBAA in a glass vial and 3-4 mL of acetone is needed to dissolve the PI. 40 mL of PEGDA at room temperature was added to this solution and vortexed several times to obtain a homogenous solution [70].

The solution was to rest for one night under the fume hood without the lid to evaporate acetone from the solution.

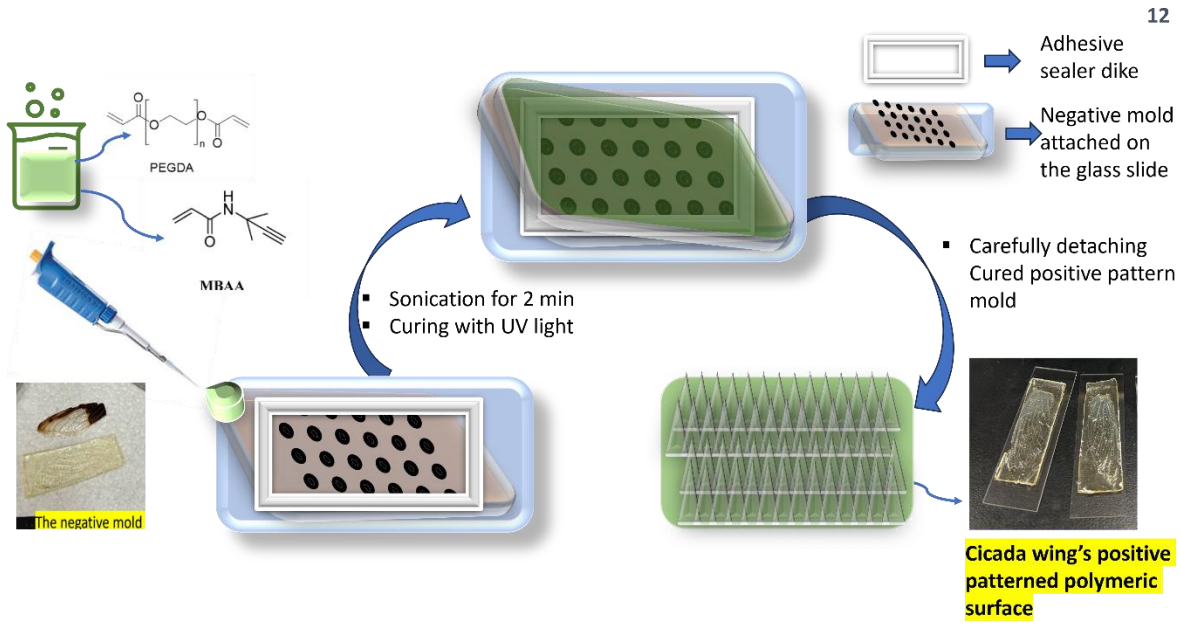


Figure 5. Preparation of MBAA functionalized PEGDA mold from PPGDA negative mold

The PPGDA negative patterned mold was kept on the top of the glass slide, adhesive sealer tape was used to create leakage-proof dikes on the edge of the PPGDA negative patterned mold. 1.5 -2 mL of MBAA functionalized PEGDA solution is drop-cast inside the dike using a pipette. Then the whole setup was kept on a Petri dish and carefully performed degassing for 2 minutes in the sonicator (BRANSON 1800). After sonication, a VWR cover glass slide was kept on the top of the dike so that no air bubbles formed.

The curing of polymer solution to fabricate the positive patterned mold was carried out in the UV crosslinker: IntelliRay 400 at 365 nm wavelength with a 10 cm distance from the light source while maintaining 100% intensity. The Exposure time for MBAA functionalized PEGDA polymer

solution was 1900 seconds. After curing, the positive patterned mold was carefully detached from the negative patterned mold with a scalpel and tweezer. PolyMBAA functionalized PEGDA positive patterned molds were cured for another 24 hours at 75˚C in the oven.

The whole fabrication process is shown in figure 5.

3.5 Click linkage between antibacterial agent and MBAA functionalized *nano* pillars

PolyMBAA modified PEGDA positive patterned samples were employed for click reaction with the antibacterial agent azido hydantoin. The samples were immersed in 60 mL tert-butyl alcohol and deionized (DI) water, where 1:1 ratio was maintained. To this solution, 160 mg of sodium ascorbate, 99-µL of aqueous $CuSO_4$ (1M), and 90-µL of Triton X-100 added. Following 10 minutes of agitation, 365 mg of C1 was added in the solution. The reaction mixture was then stirred at room temperature for 120 minutes. Subsequently, all samples were rinsed with tert-butyl alcohol and DI water for 5 minutes in an ultrasonic water bath and dried using purified air.

3.6 Chlorination of PEGDA *nano* patterned surface with *N*-Cl coating and PEGDA smooth surface with *N*-Cl coating and chlorine loading measurement

Unless noted otherwise, PEGDA *nano*-patterned surface with *N*-Cl coating and PEGDA smooth surface with *N*-Cl coating were chlorinated by immersion in 1500, 1000, or 700 ppm sodium hypochlorite solution. The samples are agitated for 30 minutes in the solution, subsequently, thoroughly rinsed with DI water to eliminate any unbound chlorine and dried with purified air.

The concentration of active chlorine on the sample surfaces was determined using iodometric titration. Three identical samples, with approximate surface dimensions of 1.5 x 1.9 cm^2, were each immersed in individual beakers containing 20 mL of 0.001 N sodium thiosulfate solution diluted with 25 mL of DI water and subjected to shaking at 100 rpm for 30 minutes. Following this, 2 mL of 5% acetic acid was added, followed by titration using 0.001 N iodine solution. The active chlorine concentration was then calculated as:

$$Active\ Chlorine\ [nmol / Cm^2] = \frac{N\ x\ \{V1 - V2\}}{2\ x\ 1000\ x\ A} \quad Equation\ 1$$

Here, V1 represents the volume in milliliters (mL) of iodine solution used for titrating blank sodium thiosulfate, V2 represents the volume in mL of iodine solution used for titrating sodium thiosulfate exposed to PEGDA nano-patterned surface with *N*-Cl coating and PEGDA smooth surface with *N*-Cl coating, N denotes the normality of the iodine solution, and A stands for the surface area of the sample in square centimeters (cm^2).

3.7 Instrumental analysis and characterization

The functionalization of MBAA on PEGDA polymeric surface was confirmed by ATR-FTIR spectra recorded on Nicolet iS10 spectrometer (Thermo Electron Corporation) and spatial resolution IR images were taken from Agilent Cary 620 FTIR microscope (64 × 64 focal plane array). The attachment of Azido hydantoin on the Alkynyl handle of MBAA by click reaction was also confirmed by ATR-FTIR spectra recorded on Nicolet iS10 spectrometer.

High-resolution Scanning electron microscope (SEM) images of *Cryptotympana aquila's* wings, negative pattern mold and MBAA functionalized PEGDA positive patterns were taken at FEI nova nanoSEM 450 at 5,10 KV under 15,000, 20,000, 35,000, 65,000, and 80,000 magnifications. All the samples were coated with 20 nm of gold−palladium (60:40) with Denton sputter coater. All SEM images were analyzed using ImageJ to measure the *nano* pillar's height, basal diameter, and tip diameter. Top-to-down images were taken and used to determine the diameter of wings and MBAA functionalized PEGDA positive mold's pillars.

The elemental composition of the chlorinated PEGDA Positive mold with MBAA was analyzed using scanning electron microscopy (SEM) associated with energy-dispersive X-ray spectroscopy (SEM/EDS). The chlorine distribution on the *nano* patterned PEGDA (MBAA functionalized) positive surface was measured using elemental mapping of EDS.

3.8 Positive charge density measurements

The positive charge density of the PEGDA *nano*-patterned surface with *N*-Cl coating and the PEGDA smooth surface with *N*-Cl coating were measured using orange II dye by binding with the positively charged side of the surfaces.

The triplicates of each sample were immersed in 2 mL of 9.7×10^{-5} M orange II dye solution in a separate breaker for 24 hours. The unbound dye solution was removed by rinsing with an excessive amount of water. The bound orange II dye was eliminated from the samples by soaking them in 1M NaOH (2 mL) solution for 30 minutes.

The UV absorbance of the solutions was taken at 483 nm after detaching the orange dye from the samples. The sample containing the positive charge density was calculated from the prepared calibration curve.

The calibration curve has been prepared from different concentrations of orange II dye solutions. Orange II dye solutions were dissolved in 1 M NaOH solution to prepare 2.5×10^{-6} M, 5×10^{-6} M, 1×10^{-5} M, 2×10^{-5} M, 4×10^{-5} M, and 8×10^{-5} M; UV absorbance was taken at 483 nm.

3.9 Water contact angle measurement

Water Contact angle (WCA) analysis on cicada wings (w), PEGDA smooth surface (P), PEGDA with nanopatterned (P_n), PEGDA with *N*-Cl coating (P_{Cl}) and PEGDA with nanopatterned with *N*-Cl coating (P_{nCl}) was performed using a ramé-hart Contact Angle Goniometers (Model No: 200-00-115, Serial No: 032404). Wing and PEGDA positive mold samples were immobilized on a glass slide with double-sided carbon tape, so they obscured the camera of the analyzer. Droplets of 2 µL of deionized water (obtained from a Milli-Q8 system from Millipore) were employed for WCA analysis.

3.10 Imaging of dead bacteria on nanopatterned PEGDA surface with *N*-Cl coating

Unless otherwise specified, the antibacterial activity of nanopatterned PEGDA surface with *N*-Cl (P_{nCl}) coating was assessed by dispersing 100 µL of *E. Coli* (3×10^5 CFU/mL) and *MRSA* (3×10^5 CFU/mL) on P_{nCl} surfaces. The samples with the dispersed bacterial solution were kept for 30 minutes in the biosafety cabinet. The bacterial solutions were pipetted out from the samples after the desired time and then washed with phosphate-buffered saline (PBS). 2.5 %

glutaraldehyde solution (prepared in 0.1 M PBS solution) was used for attaching bacteria on the top of sample surface. The samples were kept again in the biosafety cabinet for 60 minutes after the dispersion of glutaraldehyde solution on sample surfaces. The gradually increasing ethanol solution of 25%, 50%, 70%, 95% and 100% (V/V) has been used to dehydrate the fixed samples. The air-dried samples were ready to take SEM images.

3.11 Antibacterial assessment in phosphate buffered saline (PBS)

The Japanese Industrial Standard JIS Z 2801 protocol has been followed to investigate the antibacterial properties of P_{nCl} (PEGDA + Nano patterned + *N*-Cl), P_{Cl} (PEGDA + *N*-Cl), P_n (PEGDA + Nano patterned), P_s (PEGDA smooth surface - control) against *E. coli* (ATCC 25922) and *MRSA* (ATCC 33592). All the samples were cut into surface dimensions (1.9 x 1.5 cm^2) and 50 µL of $3X10^5$ CFU/mL initial bacterial suspension (*E. coli* and *MRSA*) was dispersed on the sample surface to cover the whole surface area. ALL the Samples were kept at room temperature for 3 times intervals (15 min, 30 min and 60 min). Afterward, 0.5 % of 2.45 mL of sodium thiosulphate solution was used as a stopping solution and each sample was washed with it followed by 1 min sonication and 10 second vortex. 300 µL of the solution was taken from the test tube and considered as first dilution and diluted 3 (10-fold each) times in PBS. 50 µL of serial dilution of bacterial suspension were micro plated using the drop plate technique on tryptone soya agar (TSA) plates [71]. For P_{Cl} and P_{nCl}, 1 mL of dilution 1 was taken for micro plating to improve the detection limit. All the TSA plates were kept at 37^0 C in the incubator and after 18 hours the viable bacterial colonies were counted.

$$Percent\ reduction\ of\ bacetria\ (\%) = \left(\frac{A-B}{A}\right) \times 100 \quad \textit{Equation 2}$$

$$log\ Reduction = log\frac{A}{B} \quad \textit{Equation 3}$$

where A represents the number of bacterial colonies in the control (CFU/mL), and B represents the number of bacterial colonies when exposed to the fabricated samples.

3.12 Statistical analysis

All the final fabricated samples were analyzed by the characterization experiments (including ATR-FTIR, Positive charge measurement, and Contact angle measurement), Each measurement was conducted in triplicate for technical accuracy. The data are expressed as mean ± standard deviation (SD). The surface topography of *Cryptotympana aquila's* wing features, PPGDA negative mold, and MBAA functionalized PEGDA positive mold were analyzed in Image J software. Antibacterial efficacy assessments were carried out across three independent experiments, with each experiment comprising three biological replicates and three technical replicates per sample at each time point. The results represent the mean values obtained from all independent experiments (n = 3). All the final data were analyzed by- one way ANOVA with post hoc- Tukey HSD test. *P*-value < 0.05 was considered statistically significant (https://astatsa.com/OneWay_Anova_with_TukeyHSD/).

Chapter 4: Result and Discussion

This study involves the fabrication of *nano* patterned surface, bio mimicked from cicada's wing. The *nano* spikes presented on the bio mimicked surfaces functioned with alkynyl handle and were able to facilitate the click reaction with antibacterial agent *N*-chloramine. The entire process of fabrication along with the functionalization of *nano* spike with antibacterial agent *N*-chloramine was less complicated and simple compared to the conventional method of bio mimicking of naturally occurring antibacterial surface. The surface morphology of cicada wings, negative mold and the bio mimicked positive patterned mold was analyzed using Scanning Electron Microscopy (SEM). The presence of MBAA into PEGDA network and the click reaction of C1 with the alkynyl handle of MBAA was confirmed via ATR-FTIR spectroscopy. Following this, the MBAA-functionalized PEGDA, post-click reaction with C1, was chlorinated using varying concentrations of chlorine bleach solution (1500 ppm, 1000 ppm and 700 ppm available chlorine). The quantification of active chlorine on P_{Cl} and P_{nCl} surface was performed using the iodometric titration method. Elemental mapping images were taken to check the distribution of active chlorine on P_{Cl} and P_{nCl} surface. To find the 3D dimension of *nano*patterned spikes and the exact height of *nano* spikes of the bio mimicked positive patterned mold, AFM imaging was attempted. However, the mechanical fragility of these nano-spikes impeded successful AFM imaging. This observation correlates with our finding regarding the physical interaction of these structures with bacteria. Despite *nano* spikes on the biomimetic mold being taller than the

membrane thickness of gram-negative bacteria, they failed to rupture bacterial cells due to their relative softness compared to the natural cicada wing spikes.

4.1 Functionalization of PEGDA positive surface with MBAA

PEGDA positive surface and polyMBAA functionalized PEGDA positive patterned surface were characterized using ATR-FTIR. In the spectrum of PEGDA positive pattern sample (Figure 6a) peak appeared at 2865 cm^{-1} and 860 cm^{-1} are attributed to the C–H stretching and C–H bending vibrations, respectively. The peak at 1720 cm^{-1} was observed due to the characteristic C=O stretching and the peak at 1452 cm^{-1} was attributed to the symmetric bending of the CH_2 group. The peak observed at 1349 cm^{-1} and 1295 cm^{-1} corresponded to C–O asymmetric bending. Peaks observed at 1093 cm^{-1} and 950 cm^{-1} were attributed to C–O–C stretching. Moreover. In the spectrum of PolyMBAA (figure 6b) the functionalization on the PEGDA-positive surface was confirmed using ATR- FTIR. In the spectrum of the PolyMBAA Functionalized PEGDA positive surface sample, a peak appeared at 3275 cm^{-1}, which is the characteristic alkynyl handle. This alkynyl will be utilized for a subsequent click reaction, facilitating the attachment of azido hydantoin. The peak observed at 1666 cm^{-1} at the spectrum was attributed to the amide group in the MBAA molecule, which confirmed the incorporation of MBAA in PEGDA network.

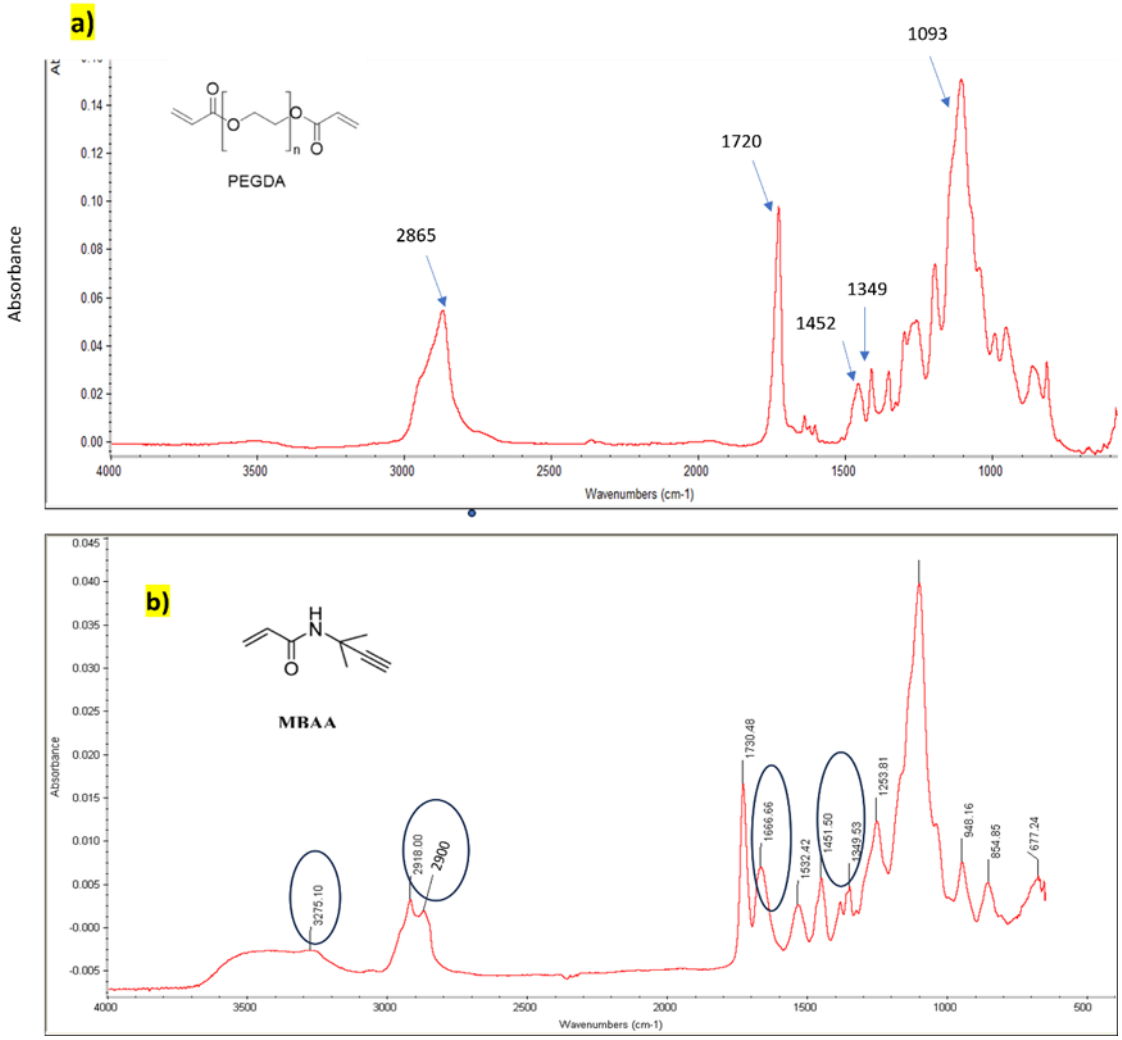


Figure 6. ATR-FTIR spectra of a) PEGDA film and b) polyMBAA functionalized PEGDA film

4.2 The topographical analysis of the *Cryptotympana aquila's* wing feature

The surface structure of Cryptotympana *aquila's* wing has been characterized by SEM imaging techniques. The Cryptotympana *aquila's* wing can be divided into two parts; one is the black part, another part considered as a transparent part. The transparent part of wings has been used in this work. The SEM images (Figure 7) confirm that the surface of the clear part of the wing consists of a hexagonal array of spikes-like structures in nanometer ranges.

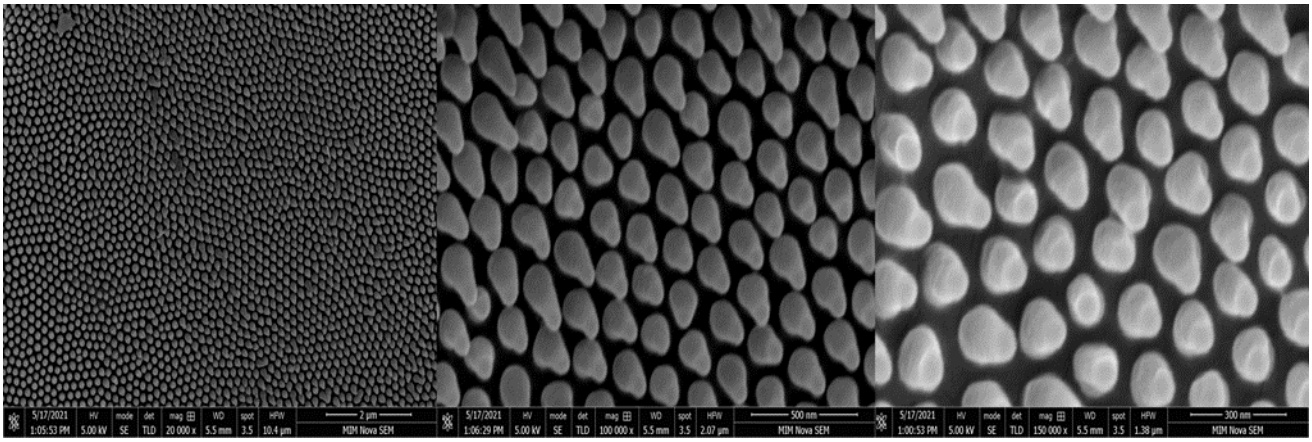


Figure 7. SEM images of Cryptotympana aqulia's wing with three different magnifications (20,000×,100,000× and 150,000×).

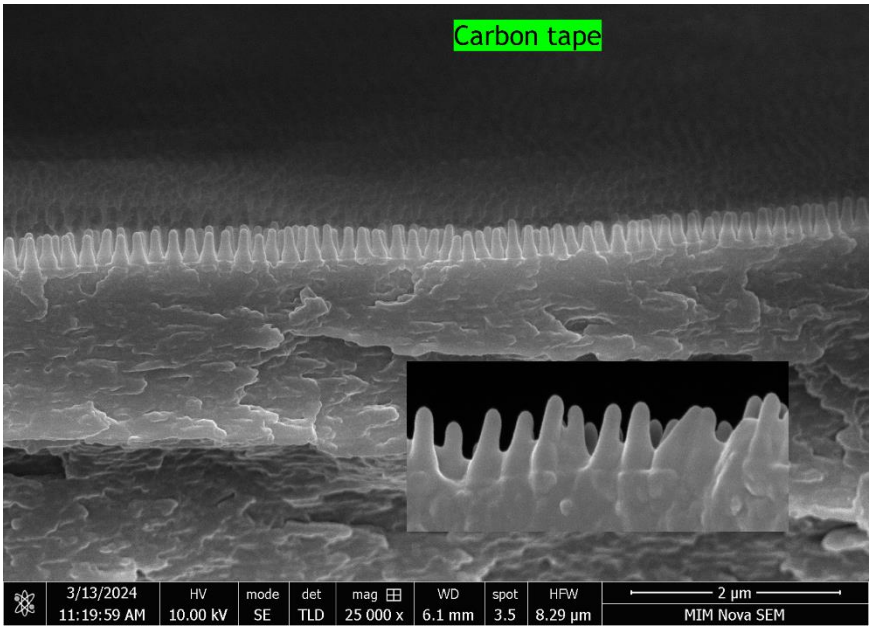


Figure 8. SEM images of Cryptotympana aqulia's wing's cross-sectional view with two different magnifications.

The cross-sectional view (figure 8) of cicada wings was taken with SEM images as well. The cicada wings emerged in liquid nitrogen for 2 minutes and cracked in the middle of wing. The cracked portion of wing was mounted with a carbon tape (facing upwards) with cubic holder

and camera was projected from the top, the height of the *nano* pillar can be measured from the cross-sectional view of cicada wings.

The frequency distribution of cicada wing's *nano* pillars' height and tips diameter is given in Figure 9, according to the distribution curve, the majority of *nano* pillars' height ranges fall within the range of 185 ± 15 nm. Very few *nano* pillars possess the lowest height with 160 ± 5 nm. *The nano* pillars are conical shaped (the tip diameter of *nano* pillars is smaller than the basal diameter of *nano* pillars), from the frequency distribution chart it is seen that most of the *nano* pillars tip diameter is in the range of 65 ± 5 nm.

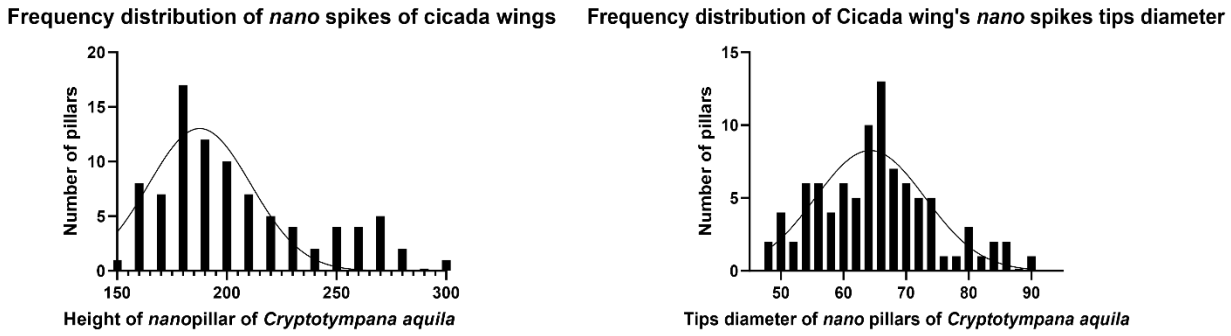


Figure 9. Frequency distribution of nano-pillars(n=100) height(nm) and tip diameter(nm) of Cryptotympana aquila's wings

4.3 Topographical analysis to analyze the fabricated negative patterned mold and MBAA functionalized PEGDA positive patterned mold

The nano ranged surface feature of fabricated negative patterned mold and MBAA functionalized PEGDA positive patterned mold was also analyzed by SEM images. The negative patterned mold was fabricated from PPGDA solution using cicada wings as a template. In Figure 10, the differences in pillar basal and tip diameters were visually highlighted, showcasing a

distinct contrast. The basal area was represented as a prominent bright white circle, while the tips area was depicted as a smaller black circle nested within the basal area.

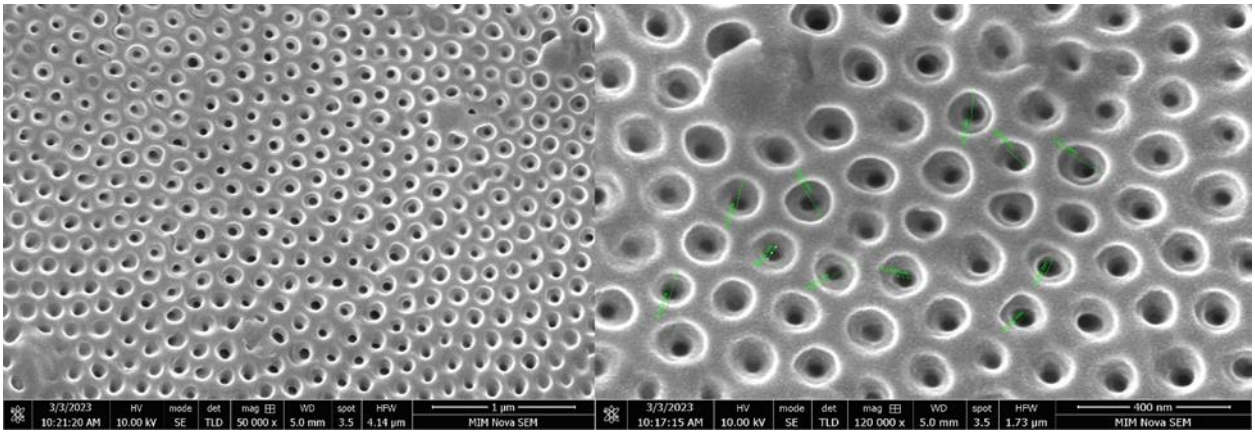


Figure 10. SEM images of negative mold prepared from PPGDA. with two different magnifications (50,000× and 120,000×)

A total number of 100 pitches have been considered to determine the average basal and tips diameter of *nano* pillars. As depicted in Figure 11, most *nano* spikes have a basal diameter and tips diameter in the range of 120 ± 5 nm and 60 ± 5 nm, respectively.

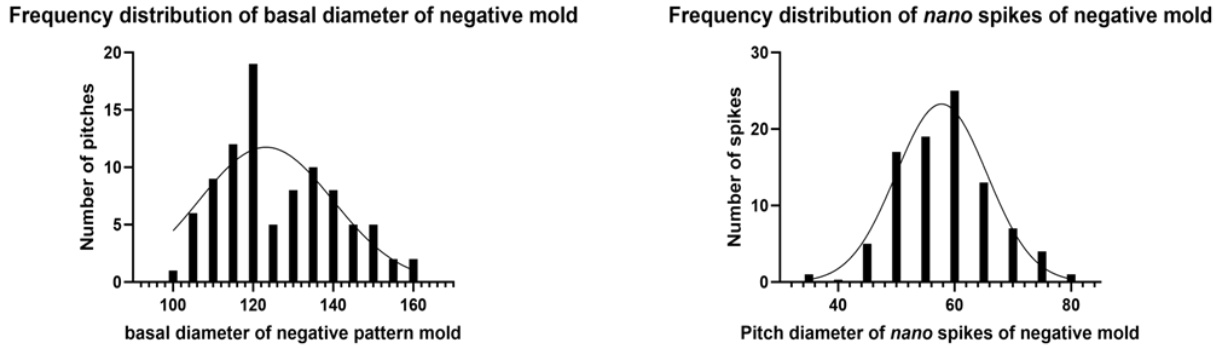


Figure 11. Frequency distribution of nano-pillars (n=100) basal diameter(nm)r and tips diameter(nm) of negative mold prepared from PPGDA.

As shown in Figure 12, SEM micrograph of fabricated MBAA functionalized PEGDA positive surface resembles the surface texture of *Cryptotympana aquila's* wings. The artificially fabricated positive surface also exhibits a hexagonal array of conical-shaped *nano* pillars on top

of it. The cross-sectional view of MBAA functionalized PEGDA positive patterned mold was taken with SEM images (figure 13). The MBAA functionalized PEGDA positive patterned mold emerged in liquid nitrogen for 7 minutes and cracked in the middle of samples. The cracked portion of sample was mounted with a carbon tape (facing upwards) with cubic holder and camera was projected from the top, the height of the *nano* pillar can be measured from the cross-sectional view of MBAA functionalized PEGDA positive patterned mold.

According to frequency distribution chart (Figure 14) majority of the *nano* pillars' height were in the range of 160 ± 10 nm and the average tip diameter of *nano* pillar is 60 ± 5 nm; which was slightly reduced from the master substrate wings.

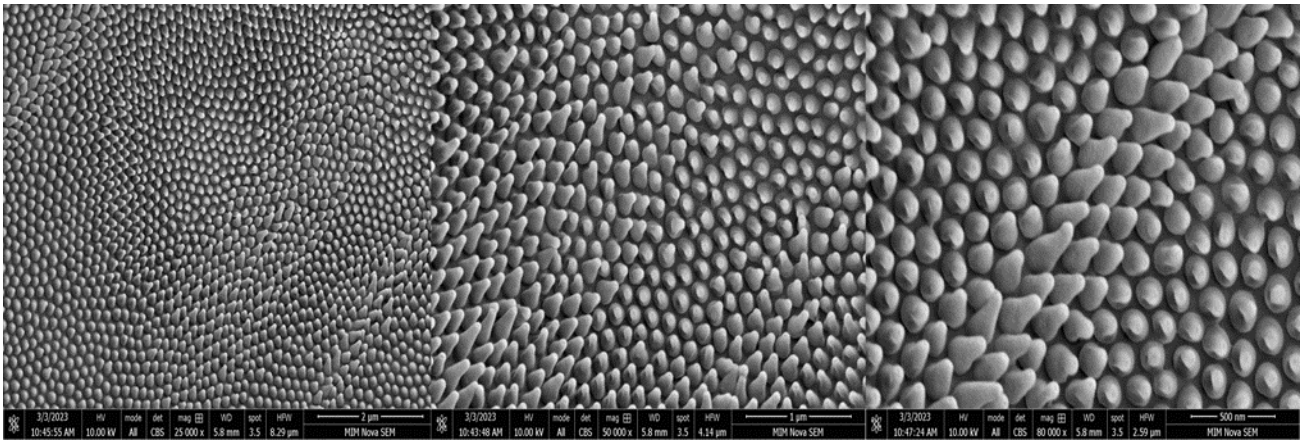


Figure 12. SEM images of Positive Patterned mold prepared from polyMBAA functionalized PEGDA. with three different magnifications (25,000×,50,000× and 80,000×)

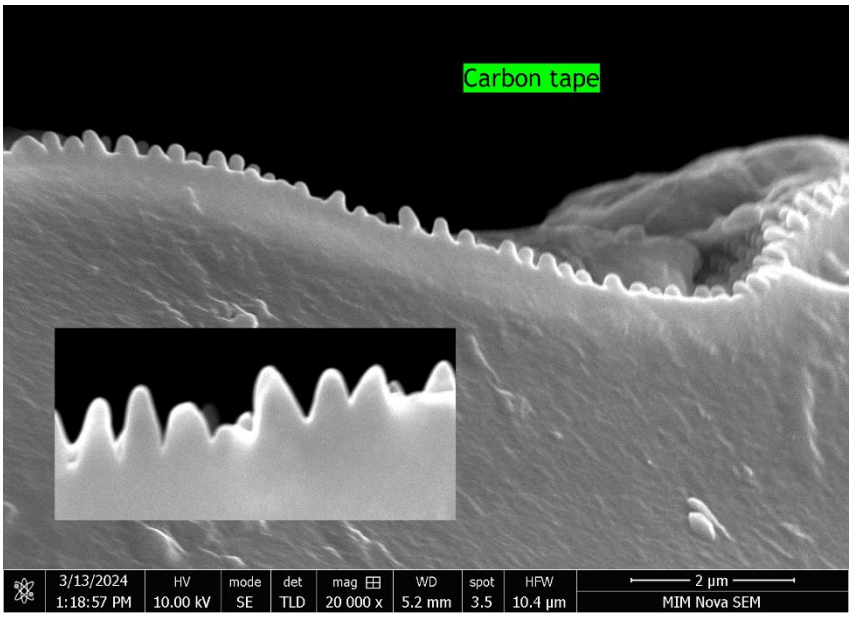


Figure 13. SEM images of Positive Patterned mold prepared from polyMBAA functionalized PEGDA's cross sectional view with two different magnifications.

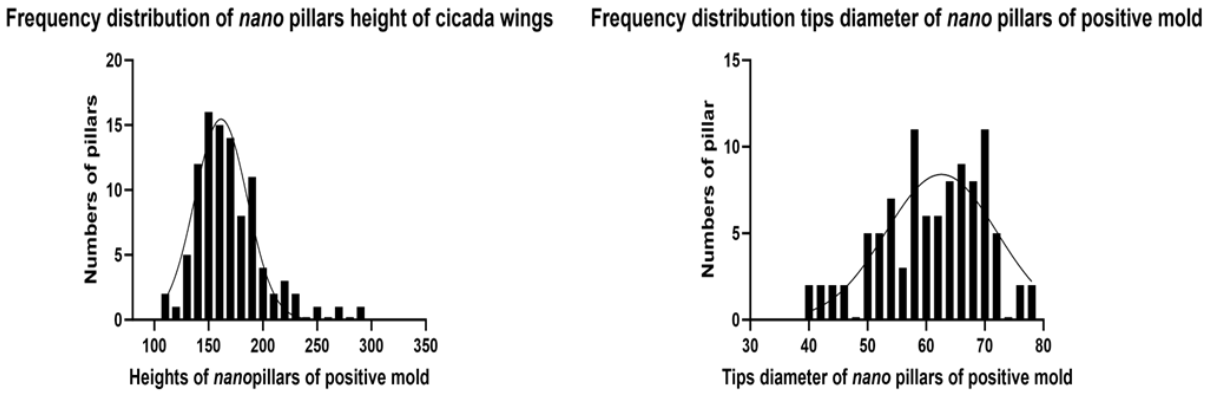


Figure 14. Frequency distribution of nano-pillars(n=100) height(nm) and tip diameter(nm) of polyMBAA functionalized PEGDA.

Table 1 provides a comprehensive summary of the heights, tip diameters, and basal diameters of *nano* spike structures across all fabricated substrates, encompassing actual wings, negative molds, and fabricated positive molds.

Table 1 Dimension of (height and tips and basal diameter) Master substrate, negative mold and positive mold

Substrate types	**Heights of *nano* spikes**	**Tips diameter of *nano* spikes**	**Basal diameter of *nano* spikes**
Cryptotympana aquila's wing	185 ± 15 nm	65 ± 5 nm	-
Negative mold made of PPDGA	-	60 ± 5 nm	120 ± 5 nm
Positive mold made of MBAA functionalized PEGDA	160 ± 10 nm	60 ± 5 nm	-

4.4 ATR-FTIR spectra for MBAA functionalized PEGDA after click reaction

The ATR-FTIR Spectra of MBAA functionalized PEGDA and MBAA functionalized PEGDA with clicked Azido Hydantoin ring (P_{nCl}) are shown in Figure 15. By comparing these two spectra, it is seen that, for P_{nCl} a shoulder peaks appeared at 1760 cm^{-1} near the sharp pick of 1708 cm^{-1} and for the symmetrical and unsymmetrical stretching of the carbonyl bonds (C=O) in C1. Moreover, there was no peak at 2122 cm^{-1} for the Azide group in P_{nCl} spectra, which refers to there was no unclicked C1 remaining on the surface.

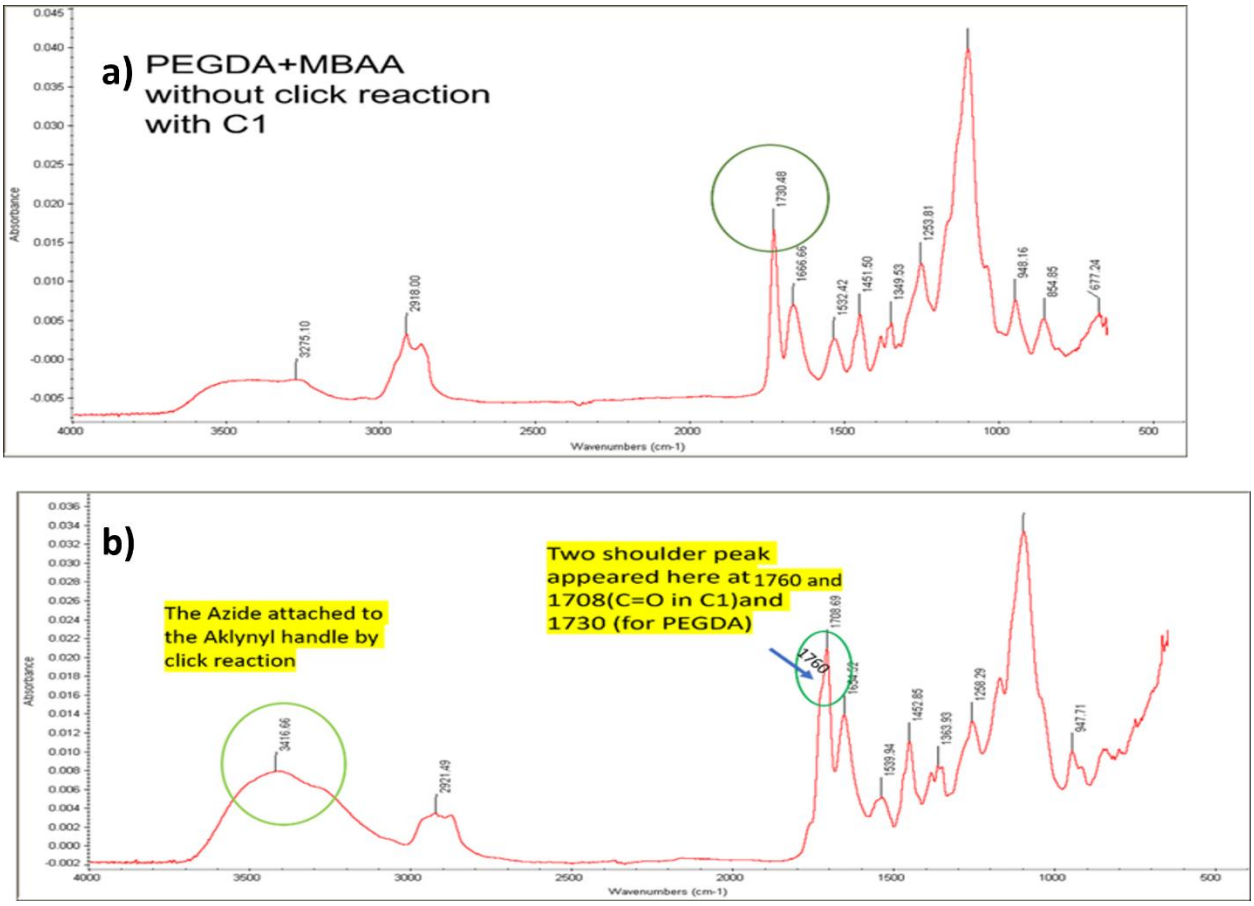


Figure 15. ATR-FTIR spectra of a) polyMBAA functionalized PEGDA film and b) polyMBAA functionalized PEGDA film after click reaction with C1.

4.5 Chlorination and chlorine loading study

The rechargeability of PEGDA smooth surface with C1 (P_{Cl}) and the evaluation of the PEGDA nano-patterned surface with C1 (P_{nCl}) involved exposing the samples to chlorination in diluted household bleach (700-1500 ppm) for 30 minutes, followed by quenching in excess sodium thiosulfate. Table 2 displays the quantitative outcomes of active chlorine loading on *N*-Cl modified samples. PEGDA smooth surface with *N*-Cl (P_{Cl}) can accommodate 41 ± 1.5 nmol/cm^2 of active chlorine with 1500 ppm of available chlorine solution whereas due to the roughness of PEGDA *nano*-patterned surface with *N*-Cl, can accommodate almost triple amounts of (110 ± 2.5 nmol/ cm^2) active chlorine on its surface by exposing same concentration of chlorine bleach solution (1500 ppm). Moreover, it's noteworthy that PnCl surfaces achieved an active chlorine loading of 42 ± 1.8 nmol/cm² when exposed to only 700 ppm of chlorine bleach solution.

Table 2 Active chlorine loading on the smooth surface with N-Cl coating and nano-patterned surface with an N-Cl precursor structure after the first time of chlorination.

concentration of available chlorine in the bleach solution used to chlorinate the sample (ppm)	active chlorine loading on the sample (nmol/cm^2)	
	Smooth surface With *N*-Cl coating	nanopatterned surface with *N*-Cl coating
1500	41 ± 1.5	110 ± 2.5
1000	-	74 ± 3.5
700	-	42 ± 1.8

4.6 Elemental mapping analysis to confirm active chlorine on the P_{nCl} surface

The *N*-Halamine precursor of the Azido hydantoin ring was converted to *N*-Cl after exposing the samples to diluted (700ppm -1500 ppm) household bleach solution. The presence of chlorine and its distribution pattern on P_{nCl} surfaces was confirmed by EDX and elemental analysis mapping, carried out in FEI NOVA nanoSEM 450. Figure 16. shows a) morphology b) EDX analysis and (c -f) elemental mapping of Chlorinated MBAA functionalized PEGDA *nano*-patterned surface.

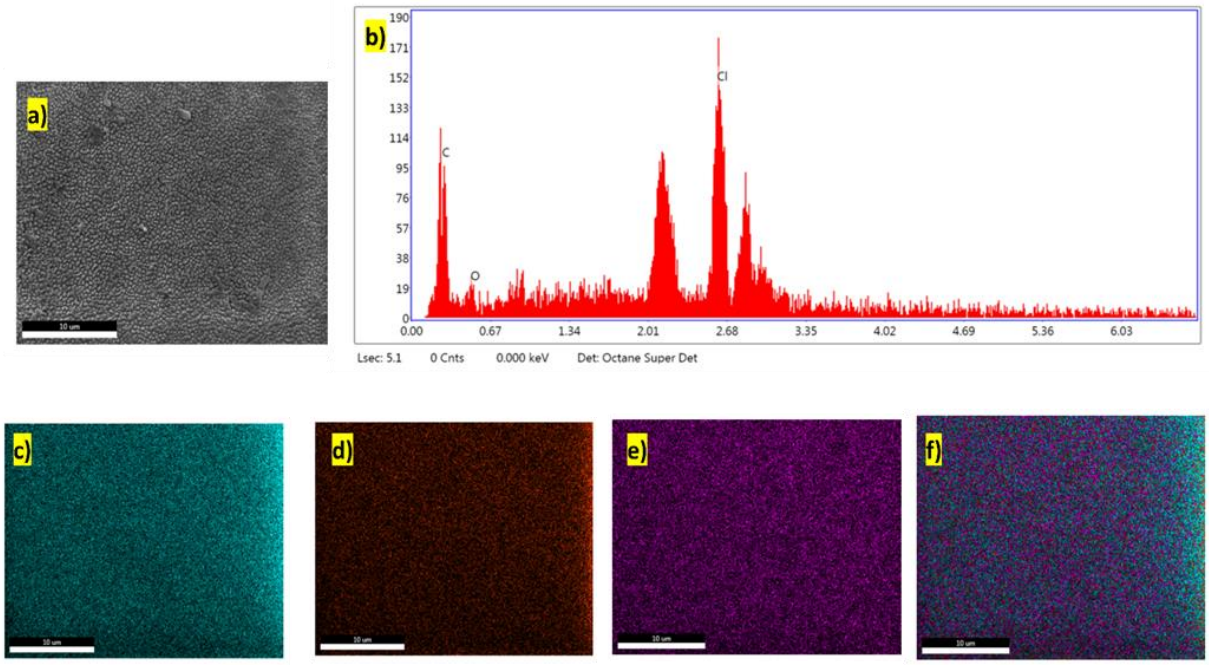


Figure 16. EDX analysis of PEGDA nano-patterned surface with C1 (b) Elemental mapping Image analysis of PEGDA nano-patterned surface with C1 C) carbon d) Oxygen e) Chlorine f) homogeneous distribution of C, O and Cl on the PnCl surface.

The sharp peak for chlorine is clearly seen in the EDX spectrum, confirming the presence of Cl and successful click reaction of C1 with MBAA functionalized PEGDA *nano*-patterned surface. Figure (16) c, d, and e, represent the elemental distribution of Carbon, Oxygen, and Chlorine on the sample surface. The purple color (representing chlorine) in Figure f) confirms the

homogeneous distribution of chlorine on P_{nCl} surface and the weight percentage of Cl is 41% (Table 3).

Table 3 Percentage of active chlorine on PEGDA nano-patterned surface with C1

Elemen	Weight	Atomic	Error %
C K	57.62	79.51	16.91
O K	1.21	1.25	99.99
ClK	41.17	19.24	5.48

To confirm the presence of Cl on the P_{nCl} surface after chlorination the cross-sectional view of sample was also analyzed with SEM-EDX, Figure 17, Spot-1 represents the area on the surface and the Cl peak was seen in EDX spectrum while there was no chlorine peak detected on the EDX spectrum of spot 2 which was the cross section of the sample.

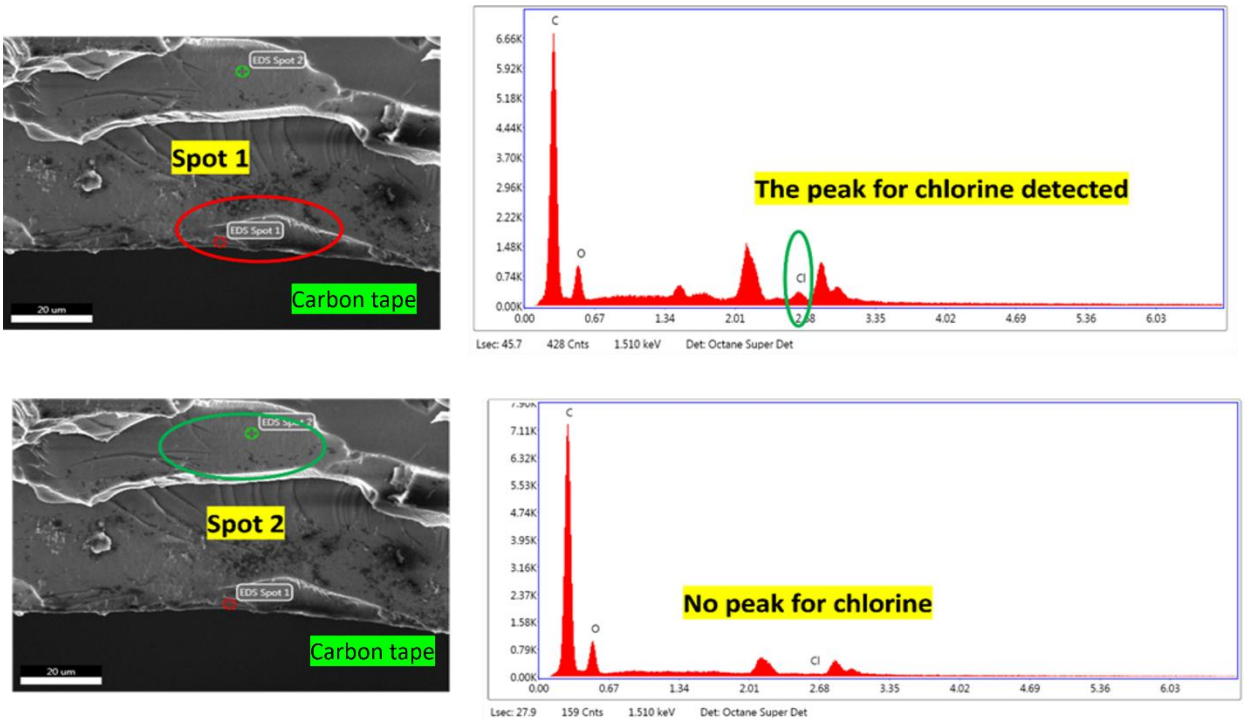


Figure 17. EDX analysis of PEGDA nano-patterned surface with C1 after chlorination: Spot 1 the surface area and Spot 2 the cross section of the sample.

4.7 Positive charge density measurement:

The positive charge density of PEGDA smooth surface and PEGDA *nano* Patterned surface was measured with a colorimetric titration experiment using Orange II after chlorination with different concentration of chlorine bleach solution. Table 4. exhibits the positive charge density for P_{Cl} and P_{nCl} samples. From the previous study it is reported that to exhibit significant antibacterial activity sample substrate should possess a positive charge density between 10^{14} to 10^{16} N^+/cm^2 on its surface [52]. From Table 4, it is seen that both P_{Cl} and P_{nCl} sample possess a positive charge density of 10^{16} N^+/cm^2. However, P_{nCl} sample possess a slightly higher positive charge than P_{Cl} sample despite chlorinating with same amount of active chlorine bleach solution.

Table 4 Positive Charge Density Measurement of PEGDA smooth surface and PEGDA nano Patterned surface after chlorination

Sample	Chlorination [Cl^+] ppm	**positive charge density (N^+/cm^2)**
P_{Cl}	1500	1.65443E+16
P_{nCl}	1500	2.23339E+16
P_{nCl}	700	1.84477E+16

4.8 Water contact angle measurements:

*Cryptotympana aquila'*s wings are hydrophobic as they exhibit the WCA 104.5^0 (WCA > 90^0). This finding matches with the Sun et al. report where they studied the wettability of 15 cicada species [73]. The Cicada wing's patterned nano spikes are hydrophobic in nature as the fatty acid and long-chain hydrocarbons are principal contributors to making up the outer epicuticle of cicada wings [74]. However, the biomimetic nano-patterned wings on PEGDA surfaces were

shown to be super hydrophilic (WCA 16.5 ±1.5), This outcome is in line with the values published by Ried et al., who mimic cicada wing's positive patterns on PEGDA surface [70] ; changes in surface chemistry is responsible for that increased hydrophilicity and water fills the air pocket around the nanospikes which results in decreased contact angle between solid and liquid interfaces [75].

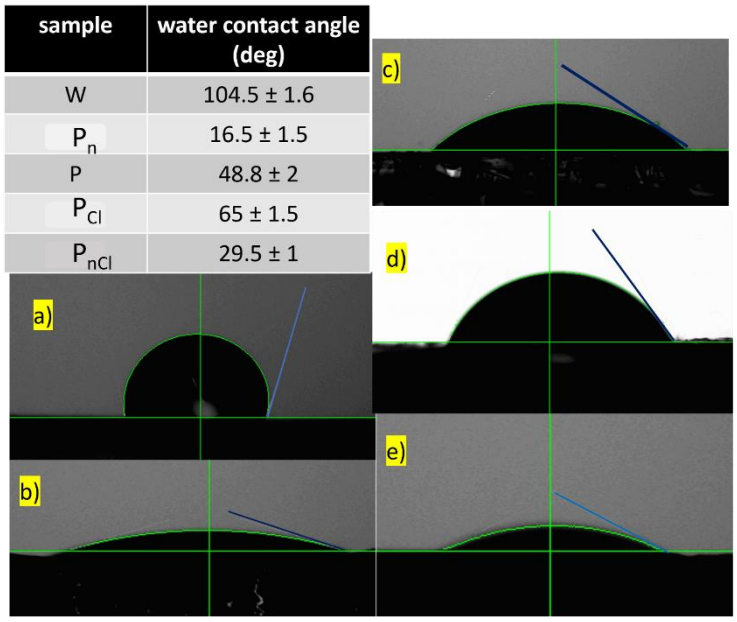


Figure 18. images of a 2 µL droplet of water on the a) wing b) wings pattern on the PEGDA surface c) PEGDA smooth surface, PEGDA with N-Cl coating, and PEGDA with N-Cl coating with the pattern as seen with the WCA instrumentation and water contact angle of all surfaces (table in upper left corner)

To evaluate the hydrophilicity the WCA of the PEGDA smooth surface (P), PEGDA with *N*-Cl coating (P_{Cl}), and PEGDA with *N*-Cl coating with pattern (P_{nCl}) were also measured (Figure 18). PEGDA smooth surfaces exhibit hydrophilicity (<90^0) with values $48.8^0 \pm 2^0$. However, the chlorinated azido hydantoin coating on the PEGDA smooth surface increased the contact angle with the values $65^0 \pm 1.5^0$. The non-polar nature of chlorinated azido hydantoin is responsible for the increased contact angle between the solid-liquid interface. Nanopatterned plays a vital

role in hydrophilicity for MBAA functionalized PEGDA with *N*-Cl coating with pattern (P_{nCl}) surface. Nano patterned increased the hydrophilicity of P_{nCl} surface despite having a non-polar chlorinated azido hydantoin coating. The increased hydrophilic nature of P_{nCl} surface with a value of $29.5^0 \pm 1^0$ facilitates the faster killing of bacterial cells.

4.9 Assessment of antibacterial activity in PBS solution

The antibacterial activity of PEGDA smooth surface (P), PEGDA with *N*-Cl coating (P_{Cl}), PEGDA with *nano*-patterned surface (P_n) and PEGDA with *N*-Cl coating with pattern (P_{nCl}) were evaluated over 3 assays each containing 3 biological replicates and 3 technical replicates against gram-negative bacteria *E. coli* (ATCC 25922) and gram-positive bacteria MRSA (ATCC 33592), Tables 5 and 6. The antibacterial activity of *N*-chloramine modified PEGDA surface is directly proportional to the total quantification of active chlorine, so; PEGDA smooth with *N*-Cl coating (P_{Cl}) and PEGDA with *N*-Cl coating with pattern (P_{nCl}) were equipped with a comparable quantity of active chlorine 41 ± 1.5 nmol/cm^2 and 42 ± 1.8 nmol/cm^2 respectively. Chlorinated PEGDA smooth surface acts as control here. Our findings revealed that P_{nCl} exhibited the most potent antibacterial activity among all samples, achieving a 100% reduction in *E. coli* (ATCC 25922) after just 15 minutes of contact. Likewise, P_{Cl} (PEGDA smooth with *N*-Cl coating) expressed 88.22% bacterial reduction of *E. coli*. after 15 minutes of contact and no surviving bacteria after 30 minutes of contact time. However, PEGDA with *nano*-patterned surface (P_n) surface had a minor antibacterial activity against *E. coli* (ATCC 25922) after 15 minutes of contact, which increased more than 90% bacterial reduction after 60 minutes of contact. The rapid antibacterial efficacy of P_{nCl} surfaces arises from the combined action of active chlorine and the

biophysical killing mechanism of nano-patterned spikes. Nevertheless, the presence of *nano*-patterned spikes endows the super hydrophilic nature of P_{nCl} surface which works synergistically with *N*-chloramine to enhance the antibacterial activity against *E. coli.* (Chlorinated PEGDA smooth Surface with *N*-Cl coating, P_{Cl} : 65 ± 1.5; Chlorinated PEGDA *nano* patterned Surface with *N*-Cl coating, P_{nCl} : 29.5 ± 1). The comparatively higher hydrophilic nature of P_{nCl} contributes to increased contact with the bacterial suspension to facilitate the faster killing of oxidative chlorine.

In comparison, P_{nCl} surfaces possessed slightly lower reactivity against gram-positive *MRSA* bacteria than gram-negative bacteria *E. coli* as presented in Figure 16. Within the first 15 minutes there was no significant bacterial reduction (MRSA) for $P_{n,}$ P_{Cl} and P_{nCl} (P values were 0.89 for $P_{n,}$-P_{Cl}, 0.08 for $P_{n,}$-P_{nCl} and 0.07 for P_{Cl}-P_{nCl}). However, the P_{nCl} and P_{Cl} surfaces demonstrate 98.7 % and 97.7 % of bacterial reduction after 30 minutes of contact. Both P_{nCl} and P_{Cl} surfaces exhibit 100 % bacterial elimination after 60 minutes of contact. The comparatively slower killing effect of P_{nCl} surfaces probably owing to the minor bactericidal potency of *nano*-spikes patterned against gram-positive bacteria. The PEGDA *nano*patterned surfaces (P_n) demonstrate 92% bacterial reduction against gram-negative bacteria *E. coli.* and only 30% bacterial reduction against gram-positive bacteria within the same time (60 mins). According to the Biophysical model of Physical damage of bacterial cells by *nano*patterned spikes, the gram-negative bacterial cell membrane is less rigid than the gram-positive bacterial cell membrane. The outer membrane of *E. coli.* Is made of lipopolysaccharides (LPS) and various types of proteins. The fabricated *nano*-patterned spikes can rapture the cell membrane of *E. coli.* as it possesses a thin layer of peptidoglycans (1-3 layers), with 3.0 nm thickness, which is thin

enough to rapture by 170 nm spikes of fabricated patterned surface and destroying the vital organs of *E. coli.* whereas due to a thicker layer of peptidoglycans (10-50 layers), gram-positive bacteria remain rigid towards *nano*-patterned spikes [47]. The outer membrane of gram-positive bacteria is made phospholipid membrane and peptidoglycan cell wall with a total thickness of 80 nm, which is rigid enough to protect the vital organ by rapturing with *nano* spikes. As the *nano* spikes are more than 80 nm, they were supposed to rapture the gram-negative bacteria's cell membrane made of peptidoglycans.

Table 5 Antibacterial efficacy of a) PEGDA smooth surface b) wings pattern on PEGDA surface c) PEGDA smooth surface with N-Cl coating, and PEGDA with N-Cl coating with the pattern against E. coli.

Samples	*Surface type*		*Chlorine loading (nmol/cm²)*	*Bacterial reduction at three contact time*					
	Physical Killing	**Chemical Killing**		**15 minutes**		**30 minutes**		**60 minutes**	
				%	**Log**	**%**	**Log**	**%**	**Log**
PEGDA smooth surface (Control)	**X**	**X**	**-**						
PEGDA with *nano* patterned surface	***nano*spikes**	**X**	**-**	**24.45**	**1.22E-01**	**73.17**	**5.71E-01**	**92.7**	**1.14E+00**
PEGDA smooth surface with *N*-Cl	**X**	***N*-Cl**	**41 ± 1.5**	**88.22**	**9.29E-01**	**100**	**5.37E+00**	**100**	**5.58E+00**
PEGDA with *nano* patterned surface with *N*-Cl	***nano*spikes**	***N*-Cl**	**42 ± 1.8**	**100**	**4.61E+00**	**100**	**5.37E+00**	**100**	**5.58E+00**

Figure 19. represents Log Reduction P_n, P_{Cl}, and P_{nCl} compared to Control at 3 different time points for *E. coli.* and MRSA. [a,b,c] The presence of distinct letters within each groups serves as an indicator of significant differences ($P < 0.05$), and the absence of letters within the group or the presence of identical letters in the data signifies that the observed difference is not significant ($P > 0.05$).

Table 6 Antibacterial efficacy of a) PEGDA smooth surface b) wings pattern on PEGDA surface c) PEGDA smooth surface with N-Cl coating, and PEGDA with N-Cl coating with the pattern against MRSA

Samples	*Surface type*		*Chlorine loading (nmol/cm²)*	*Bacterial reduction at three contact time*					
	Physical Killing	**Chemical Killing**		**15 minutes**		**30 minutes**		**60 minutes**	
				%	**Log**	**%**	**Log**	**%**	**Log**
PEGDA smooth surface (Control)	**X**	**X**	**-**						
PEGDA with *nano* patterned surface	***nano*spikes**	**X**	**-**	**22.4**	**1.10E-01**	**24.7**	**1.24E-01**	**30.8**	**1.60E-01**
PEGDA smooth surface with *N*-Cl	**X**	***N*-Cl**	**41 ± 1.5**	**24.5**	**1.23E-01**	**97.7**	**1.64E+00**	**100**	**4.96E+00**
PEGDA with *nano* patterned surface with *N*-Cl	***nano*spikes**	***N*-Cl**	**42 ± 1.8**	**49.8**	**2.55E-01**	**98.76**	**1.91E+00**	**100**	**4.96E+00**

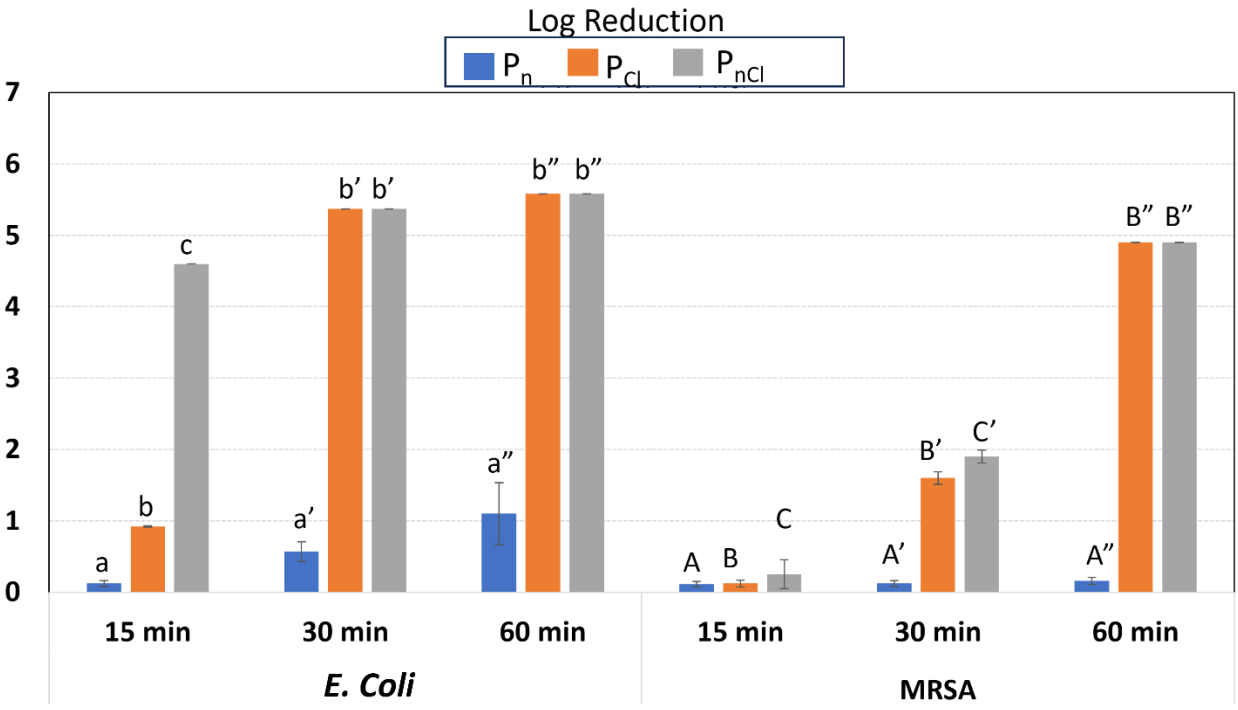


Figure 19. Log Reduction P_n, P_{Cl}, and P_{nCl} compared to Control at 3 different time points for E. coli and MRSA (different alphabet indicates significant difference within each group and P-value < 0.01).

4.10 SEM micrographs of bacteria on the chlorinated P_{nCl} surface

Both gram-negative bacteria *E. coli* (ATCC 25922) and gram-positive bacteria MRSA (ATCC 33592) on the surface of chlorinated PEGDA *nano*-patterned with *N*-Cl coating were imaged using SEM. Among all samples, the P_{nCl} demonstrated the best antibacterial activity, so we chose this sample to shine on bacterial morphology after damage. Figure 20, illustrates the damage to *E. coli* on the P_{nCl} surface, resulting from membrane disruption due to contact with quaternary ammonium compounds and *N*-Cl within the coating, alongside physical damage caused by *nano*-spiked pillars. In contrast, damage of MRSA on top of the P_{nCl} surface is caused by the diffusion of oxidative chlorine on bacterial surfaces.

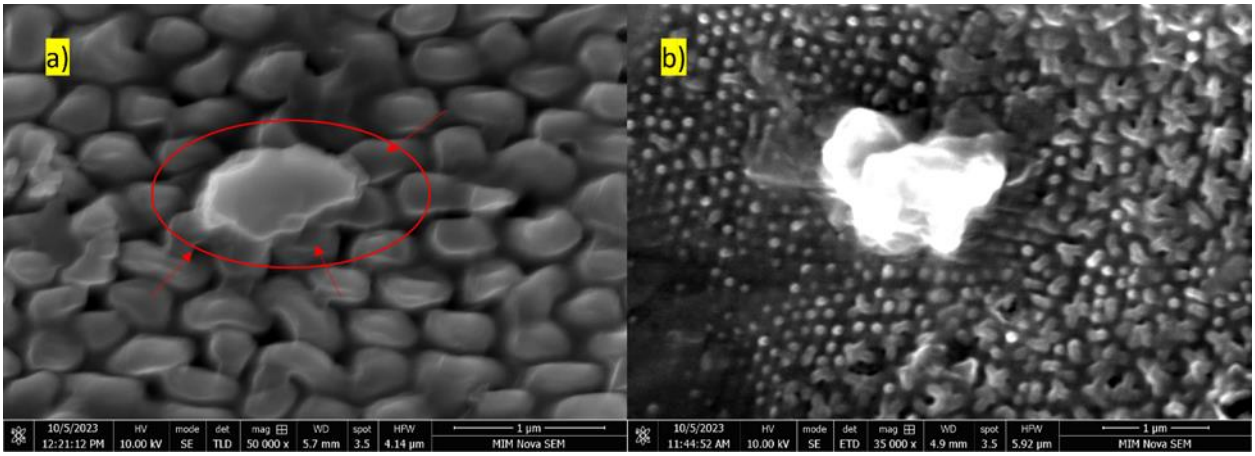


Figure 20. Cell damages caused by PEGDA with N-Cl coating with pattern (PnCl) E. coli (L) and MRSA (R)

Chapter 5: Conclusions

The fabrication of the cicada wing-inspired biomimetic contact active biocidal surface along with a clickable antibacterial agent was achieved by simplified replication techniques using UV cross-linkable polymer. This study demonstrates the successful fabrication of contact active biocidal surface by merging the contact active physical killing approach along with the contact killing chemical killing approach. According to Reid et al. research study, the primary mold made from PPG polymer has lowered Interfacial adhesion, higher chain length, and lower Young's modulus compared to PEG secondary molds. This allows the successful demolding of the final fabricated from the negative mold without losing the *nano*-patterned feature from the secondary surface [70]. An essential component for the success of this endeavor was the functionalization of the secondary mold (made of PEGDA) *nano*-patterned features with MBAA monomer to endow click reaction sites on the surface topography. Grafting of MBAA monomer on the PEGDA polymer network initiates changes in interfacial adhesion along with young modulus, making it difficult to de-mold from the primary mold without losing its *nano*-patterned features. The proper mixing ratio of MBAA monomer in PEGDA polymer, and fine-tuning of curing time for both primary mold and MBAA functionalized secondary mold allows successful demolding without hampering its surface topography confirmed by SEM analysis. The introduction of an alkynyl handle on UV-curable polymer can be used to develop a stable, rechargeable, and versatile click reaction site on the biomimetic antibacterial surface. Numerous research investigations have demonstrated that *N*-chloramines exhibit potent biocidal activity against a variety of bacteria, fungi, and viruses.[76]–[78]. After attaching *N*-chloramine by click reaction on the fabricated *nano*-patterned surfaces, it exhibits significant antibacterial activity by showing a 100% reduction of *E.*

coli. Within 15 minutes of contact and a 100% reduction of MRSA within 60 minutes of contact. Finally, this research study demonstrates that the cicada wings inspired artificially fabricated surfaces along with clickable antibacterial agent *N*-chloramine were able to exhibit enhanced antibacterial efficacy against *E. coli* and MRSA.

Chapter 6: Future Work

In this study, the antibacterial efficacy of the final fabricated surface is based on quaternized *N*-chloramine and bio-mimicked cicada wings patterned on the polymeric surface. The bio-mimicked cicada wing pattern made the fabricated surface super hydrophilic and increased the amount of active chlorine and clicked antibacterial agent. *N*-chloramine also influenced the positive charge density and the quantitative amount of active chlorine. The above-mentioned factors enhanced the antibacterial efficacy against gram-positive and gram-negative bacteria.

The physical killing approach due the *nano* spikes is much slower compared to the natural antibacterial surface, cicada wings as the fabricated *nano* pillar's tip is not strong enough to rapture bacterial cell wall. The mechanical strength of *nano* pillar tips can be increased by incorporating reinforcement element to the polymeric network. The incorporation of such reinforcement element to the polymeric network to strengthen the "*nano*-pillar's tip" can be studied in future work.

The nano-pillar tips with their patterned structure can be treated with newly quaternized *N*-chloramine molecules, which bear multiple positive charges and additional N-H bonds. This modification has the potential to enhance the antibacterial effectiveness of the patterned polymeric surface. Click reactions with such antibacterial agent can be explored in future research.

More study is needed for finding the stability of coating during the chlorination along with acidic and basic environment.

The final fabricated surface: PEGDA with *N*-Cl coating with pattern was assessed with Gram-negative *E. coli* and Gram-positive *MRSA*. In Health care sector, there exists a broader array of microorganisms including viruses and fungi. It is recommended that more research can be done to challenge the PEGDA with *N*-Cl coating with pattern surface by a wider spectrum of microorganisms and bacteria including *Listeria monocytogenes.*

.

References

[1] R. M. Klevens, J. R. Edwards, C. L. Richards Jr, T. C. Horan, R. P. Gaynes, D. A. Pollock, and D. M. Cardo. “Estimating Health Care-Associated Infections and Deaths in U.S. Hospitals, 2002,” *Public Health Reports*, vol. 122, no. 2, pp. 160–166, Mar. 2007, doi: 10.1177/003335490712200205.

[2] S. Ferraris and S. Spriano, “Antibacterial titanium surfaces for medical implants,” *Materials Science and Engineering: C*, vol. 61, pp. 965–978, Apr. 2016, doi: 10.1016/j.msec.2015.12.062.

[3] H. H. Tuson and D. B. Weibel, “Bacteria–surface interactions,” *Soft Matter*, vol. 9, no. 17, p. 4368, 2013, doi: 10.1039/c3sm27705d.

[4] A. S. Lynch and G. T. Robertson, “Bacterial and Fungal Biofilm Infections,” *Annu Rev Med*, vol. 59, no. 1, pp. 415–428, Feb. 2008, doi: 10.1146/annurev.med.59.110106.132000.

[5] E. Khaskin, T. Fadida, Y. Kroupitski, M. Shemesh, D. A. Cristaldi, A. Gulino, and E. Poverenov, “A contact active bactericidal stainless steel via a sustainable process utilizing electrodeposition and covalent attachment in water,” *Green Chemistry*, vol. 17, no. 4, pp. 2344–2347, 2015, doi: 10.1039/C4GC02326A.

[6] P. Elena and K. Miri, “Formation of contact active antimicrobial surfaces by covalent grafting of quaternary ammonium compounds,” *Colloids Surf B Biointerfaces*, vol. 169, pp. 195–205, Sep. 2018, doi: 10.1016/j.colsurfb.2018.04.065.

[7] K. Glinel, A. M. Jonas, T. Jouenne, J. Leprince, L. Galas, and W. T. S. Huck, “Antibacterial and Antifouling Polymer Brushes Incorporating Antimicrobial Peptide,” *Bioconjug Chem*, vol. 20, no. 1, pp. 71–77, Jan. 2009, doi: 10.1021/bc800280u.

[8] F. Costa, I. F. Carvalho, R. C. Montelaro, P. Gomes, and M. C. L. Martins, “Covalent immobilization of antimicrobial peptides (AMPs) onto biomaterial surfaces,” *Acta Biomater*, vol. 7, no. 4, pp. 1431–1440, Apr. 2011, doi: 10.1016/j.actbio.2010.11.005.

[9] B. Demir, R. Broughton, M. Qiao, T.-S. Huang, and S. Worley, “N-Halamine Biocidal Materials with Superior Antimicrobial Efficacies for Wound Dressings,” *Molecules*, vol. 22, no. 10, p. 1582, Sep. 2017, doi: 10.3390/molecules22101582.

[10] S. B. Barnela, S. D. Worley, and D. E. Williams, “Syntheses and Antibacterial Activity of New N-Halamine Compounds,” *J Pharm Sci*, vol. 76, no. 3, pp. 245–247, Mar. 1987, doi: 10.1002/jps.2600760314.

[11] R. Kaur and S. Liu, “Antibacterial surface design – Contact kill,” *Prog Surf Sci*, vol. 91, no. 3, pp. 136–153, 2016, doi: 10.1016/j.progsurf.2016.09.001.

[12] C. Ning, L. Li, S. Logsetty, S. Ghanbar, M. Guo, W. Ens, and S. Liu, “Enhanced antibacterial activity of new ‘composite’ biocides with both N-chloramine and quaternary ammonium moieties,” *RSC Adv*, vol. 5, no. 114, pp. 93877–93887, 2015, doi: 10.1039/c5ra15714e.

[13] A. Tripathy, P. Sen, B. Su, and W. H. Briscoe, “Natural and bioinspired nanostructured bactericidal surfaces,” *Adv Colloid Interface Sci*, vol. 248, pp. 85–104, 2017, doi: 10.1016/j.cis.2017.07.030.

[14] S. Pogodin, J. Hasan, V. A. Baulin, H. K. Webb, V. K. Truong, V. Boshkovikj, C. J. Fluke, G. S. Watson, and E. P. Ivanova, “Biophysical Model of Bacterial Cell Interactions with Nanopatterned Cicada Wing Surfaces,” *Biophys J*, vol. 104, no. 4, pp. 835–840, Feb. 2013, doi: 10.1016/j.bpj.2012.12.046.

[15] X. Li, “Bactericidal mechanism of nanopatterned surfaces,” *Physical Chemistry Chemical Physics*, vol. 18, no. 2, pp. 1311–1316, 2016, doi: 10.1039/C5CP05646B.

[16] J. Hasan, H. K. Webb, V. K. Truong, S. Pogodin, V. A. Baulin, G. S. Watson, J. A. Watson, R. J. Crawford and E. P. Ivanova, “Selective bactericidal activity of nanopatterned superhydrophobic cicada Psaltoda claripennis wing surfaces,” *Appl Microbiol Biotechnol*, vol. 97, no. 20, pp. 9257–9262, Oct. 2013, doi: 10.1007/s00253-012-4628-5.

[17] E. P. Ivanova, J. Hasan, H. K. Webb, G. Gervinskas, S. Juodkazis, V. K. Truong, A. H. F. Wu, and R. F. Crawford, “Bactericidal activity of black silicon,” *Nat Commun*, vol. 4, no. 1, p. 2838, Dec. 2013, doi: 10.1038/ncomms3838.

[18] S. J. Lam, N. M. O'Brien-Simpson, N. Pantarat, A. Sulistio, E. H. H. Wong, Y. Y. Chen, J. C. Lenzo, and G. G. Qiao, “Combating multidrug-resistant Gram-negative bacteria with structurally nanoengineered antimicrobial peptide polymers,” *Nat Microbiol*, vol. 1, no. 11, p. 16162, Nov. 2016, doi: 10.1038/nmicrobiol.2016.162.

[19] N. M. Milović, J. Wang, K. Lewis, and A. M. Klibanov, “ImmobilizedN-alkylated polyethylenimine avidly kills bacteria by rupturing cell membranes with no resistance developed,” *Biotechnol Bioeng*, vol. 90, no. 6, pp. 715–722, Jun. 2005, doi: 10.1002/bit.20454.

[20] J. C. Tiller, C.-J. Liao, K. Lewis, and A. M. Klibanov, “Designing surfaces that kill bacteria on contact,” *Proceedings of the National Academy of Sciences*, vol. 98, no. 11, pp. 5981–5985, May 2001, doi: 10.1073/pnas.111143098.

[21] M. Ignatova, S. Voccia, B. Gilbert, N. Markova, P. S. Mercuri, M. Galleni, V. Sciannamea, S. Lenoir and R. Jérôme, “Synthesis of Copolymer Brushes Endowed with Adhesion to Stainless Steel Surfaces and Antibacterial Properties by Controlled Nitroxide-Mediated Radical Polymerization,” *Langmuir*, vol. 20, no. 24, pp. 10718–10726, Nov. 2004, doi: 10.1021/la048347t.

[22] F. Hui and C. Debiemme-Chouvy, “Antimicrobial N -Halamine Polymers and Coatings: A Review of Their Synthesis, Characterization, and Applications,” *Biomacromolecules*, vol. 14, no. 3, pp. 585–601, Mar. 2013, doi: 10.1021/bm301980q.

[23] M. V. Graham, A. P. Mosier, T. R. Kiehl, A. E. Kaloyeros, and N. C. Cady, “Development of antifouling surfaces to reduce bacterial attachment,” *Soft Matter*, vol. 9, no. 27, p. 6235, 2013, doi: 10.1039/c3sm50584g.

[24] R. Arnitz, B. Sarg, H. W. Ott, A. Neher, H. Lindner, and M. Nagl, “Protein sites of attack ofN-chlorotaurine inEscherichia coli,” *Proteomics*, vol. 6, no. 3, pp. 865–869, Feb. 2006, doi: 10.1002/pmic.200500054.

[25] L. Cen, K. G. Neoh, and E. T. Kang, “Surface Functionalization Technique for Conferring Antibacterial Properties to Polymeric and Cellulosic Surfaces,” *Langmuir*, vol. 19, no. 24, pp. 10295–10303, Nov. 2003, doi: 10.1021/la035104c.

[26] W. Gottardi and M. Nagl, “N-chlorotaurine, a natural antiseptic with outstanding tolerability,” *Journal of Antimicrobial Chemotherapy*, vol. 65, no. 3, pp. 399–409, Mar. 2010, doi: 10.1093/jac/dkp466.

[27] A. Dong, Y. J. Wang, Y. Gao, T. Gao, and G. Gao, “Chemical Insights into Antibacterial N-Halamines,” *Chem Rev*, vol. 117, no. 6, pp. 4806–4862, 2017, doi: 10.1021/acs.chemrev.6b00687.

[28] M. C. Jennings, K. P. C. Minbiole, and W. M. Wuest, “Quaternary Ammonium Compounds: An Antimicrobial Mainstay and Platform for Innovation to Address Bacterial Resistance,” *ACS Infect Dis*, vol. 1, no. 7, pp. 288–303, Jul. 2015, doi: 10.1021/acsinfecdis.5b00047.

[29] Y. Jiao, L. Niu, S. Ma, J. Li, F. R. Tay, and J. Chen, “Quaternary ammonium-based biomedical materials: State-of-the-art, toxicological aspects and antimicrobial resistance,” *Prog Polym Sci*, vol. 71, pp. 53–90, Aug. 2017, doi: 10.1016/j.progpolymsci.2017.03.001.

[30] O. Bouloussa, F. Rondelez, and V. Semetey, “A new, simple approach to confer permanent antimicrobial properties to hydroxylated surfaces by surface functionalization,” *Chemical Communications*, no. 8, p. 951, 2008, doi: 10.1039/b716026g.

[31] B. Gottenbos, H. C. van der Mei, F. Klatter, P. Nieuwenhuis, and H. J. Busscher, “In vitro and in vivo antimicrobial activity of covalently coupled quaternary ammonium silane coatings on silicone rubber,” *Biomaterials*, vol. 23, no. 6, pp. 1417–1423, Mar. 2002, doi: 10.1016/S0142-9612(01)00263-0.

[32] J. Huang, R. R. Koepsel, H. Murata, W. Wu, S. B. Lee, T. Kowalewski, A. J. Russell, and K. Matyjaszewski, “Nonleaching Antibacterial Glass Surfaces via ‘Grafting Onto’: The Effect of the Number of Quaternary Ammonium Groups on Biocidal Activity,” *Langmuir*, vol. 24, no. 13, pp. 6785–6795, Jul. 2008, doi: 10.1021/la8003933.

[33] R. Kügler, O. Bouloussa, and F. Rondelez, “Evidence of a charge-density threshold for optimum efficiency of biocidal cationic surfaces,” *Microbiology (N Y)*, vol. 151, no. 5, pp. 1341–1348, May 2005, doi: 10.1099/mic.0.27526-0.

[34] A. M. Bieser and J. C. Tiller, “Mechanistic Considerations on Contact-Active Antimicrobial Surfaces with Controlled Functional Group Densities,” *Macromol Biosci*, vol. 11, no. 4, pp. 526–534, Apr. 2011, doi: 10.1002/mabi.201000398.

[35] L. A. Asri, M. Crismaru, S. Roest, Y. Chen, O. Ivashenko, P. Rudolf, J. C. Tiller, H. C. van der Mei, T. J. Loontjens, and H. J. Busscher, “A Shape-Adaptive, Antibacterial-Coating of Immobilized Quaternary-Ammonium Compounds Tethered on Hyperbranched Polyurea and its Mechanism of Action,” *Adv Funct Mater*, vol. 24, no. 3, pp. 346–355, Jan. 2014, doi: 10.1002/adfm.201301686.

[36] H. Murata, R. R. Koepsel, K. Matyjaszewski, and A. J. Russell, “Permanent, non-leaching antibacterial surfaces—2: How high density cationic surfaces kill bacterial cells,” *Biomaterials*, vol. 28, no. 32, pp. 4870–4879, Nov. 2007, doi: 10.1016/j.biomaterials.2007.06.012.

[37] L. Caillier, E. T. de Givenchy, R. Levy, Y. Vandenberghe, S. Géribaldi, and F. Guittard, “Synthesis and antimicrobial properties of polymerizable quaternary ammoniums,” *Eur J Med Chem*, vol. 44, no. 8, pp. 3201–3208, Aug. 2009, doi: 10.1016/j.ejmech.2009.03.031.

[38] J. Hasan and K. Chatterjee, “Recent advances in engineering topography mediated antibacterial surfaces,” *Nanoscale*, vol. 7, no. 38, pp. 15568–15575, 2015, doi: 10.1039/C5NR04156B.

[39] X. Li, “Bactericidal mechanism of nanopatterned surfaces,” *Physical Chemistry Chemical Physics*, vol. 18, no. 2, pp. 1311–1316, 2016, doi: 10.1039/C5CP05646B.

[40] A. Jaggessar, H. Shahali, A. Mathew, and P. K. D. V. Yarlagadda, “Bio-mimicking nano and micro-structured surface fabrication for antibacterial properties in medical implants,” *J Nanobiotechnology*, vol. 15, no. 1, p. 64, Dec. 2017, doi: 10.1186/s12951-017-0306-1.

[41] D. P. Linklater, S. Juodkazis, and E. P. Ivanova, “Nanofabrication of mechano-bactericidal surfaces,” *Nanoscale*, vol. 9, no. 43, pp. 16564–16585, 2017, doi: 10.1039/C7NR05881K.

[42] E. P. Ivanova, J. Hasan, H. K. Webb, V. K. Truong, G. S. Watson, J. A. Watson, V. A. Baulin, S. Pogodin, J. Y. Wang, M. J. Tobin, and C. Löbbe, “Natural Bactericidal Surfaces: Mechanical Rupture of Pseudomonas aeruginosa Cells by Cicada Wings,” *Small*, vol. 8, no. 16, pp. 2489–2494, Aug. 2012, doi: 10.1002/smll.201200528.

[43] T. Diu, N. Faruqui, T. Sjöström, B. Lamarre, H. F. Jenkinson, B. Su, and M. G. Ryadnov “Cicada-inspired cell-instructive nanopatterned arrays,” *Sci Rep*, vol. 4, no. 1, p. 7122, Nov. 2014, doi: 10.1038/srep07122.

[44] M. Sun, G. S. Watson, Y. Zheng, J. A. Watson, and A. Liang, “Wetting properties on nanostructured surfaces of cicada wings,” *Journal of Experimental Biology*, vol. 212, no. 19, pp. 3148–3155, Oct. 2009, doi: 10.1242/jeb.033373.

[45] E. P. Ivanova, J. Hasan, H. K. Webb, V. K. Truong, G. S. Watson, J. A. Watson, V. A. Baulin, S. Pogodin, J. Y. Wang, M. J. Tobin, and C. Löbbe, “Natural Bactericidal Surfaces: Mechanical Rupture of *Pseudomonas aeruginosa* Cells by Cicada Wings,” *Small*, vol. 8, no. 16, pp. 2489–2494, Aug. 2012, doi: 10.1002/smll.201200528.

[46] J. Hasan, H. K. Webb, V. K. Truong, S. Pogodin, V. A. Baulin, G. S. Watson, J. A. Watson, R. J. Crawford and E. P. Ivanova, “Selective bactericidal activity of nanopatterned superhydrophobic cicada Psaltoda claripennis wing surfaces,” *Appl Microbiol Biotechnol*, vol. 97, no. 20, pp. 9257–9262, Oct. 2013, doi: 10.1007/s00253-012-4628-5.

[47] A. Jaggessar, H. Shahali, A. Mathew, and P. K. D. V. Yarlagadda, “Bio-mimicking nano and micro-structured surface fabrication for antibacterial properties in medical implants,” *J Nanobiotechnology*, vol. 15, no. 1, p. 64, Dec. 2017, doi: 10.1186/s12951-017-0306-1.

[48] M. Arnoldi, M. Fritz, E. Bäuerlein, M. Radmacher, E. Sackmann, and A. Boulbitch, “Bacterial turgor pressure can be measured by atomic force microscopy,” *Phys Rev E*, vol. 62, no. 1, pp. 1034–1044, Jul. 2000, doi: 10.1103/PhysRevE.62.1034.

[49] X. Li, “Bactericidal mechanism of nanopatterned surfaces,” *Physical Chemistry Chemical Physics*, vol. 18, no. 2, pp. 1311–1316, 2016, doi: 10.1039/C5CP05646B.

[50] L. C. Hsu, J. Fang, D. A. Borca-Tasciuc, R. W. Worobo, and C. I. Moraru, “Effect of Micro- and Nanoscale Topography on the Adhesion of Bacterial Cells to Solid Surfaces,” *Appl Environ Microbiol*, vol. 79, no. 8, pp. 2703–2712, Apr. 2013, doi: 10.1128/AEM.03436-12.

[51] T. W. Kim, “Assessment of Hydro/Oleophobicity for Shark Skin Replica with Riblets,” *J Nanosci Nanotechnol*, vol. 14, no. 10, pp. 7562–7568, Oct. 2014, doi: 10.1166/jnn.2014.9570.

[52] M. R. Kazemian, L. Wang, and S. Liu, “Engineering Rechargeable Antibacterial Coatings on Stainless Steel for Efficient Inactivation of Pathogenic Bacteria in the Presence of Organic Matter,” *ACS Appl Bio Mater*, vol. 2, no. 11, pp. 5021–5031, Nov. 2019, doi: 10.1021/acsabm.9b00721.

[53] L. Li, N. Zhao, and S. Liu, “Versatile surface biofunctionalization of poly(ethylene terephthalate) by interpenetrating polymerization of a butynyl monomer followed by ‘Click Chemistry,’” *Polymer (Guildf)*, vol. 53, no. 1, pp. 67–78, Jan. 2012, doi: 10.1016/j.polymer.2011.11.036.

[54] M. G. F. K. B. S. C. Kolb, “Click Chemistry: Diverse Chemical Function from a Few Good Reactions”.

[55] Y. Su, J. Ge, B. Zhu, Y.-G. Zheng, Q. Zhu, and S. Q. Yao, “Target identification of biologically active small molecules via in situ methods,” *Curr Opin Chem Biol*, vol. 17, no. 5, pp. 768–775, Oct. 2013, doi: 10.1016/j.cbpa.2013.06.005.

[56] R. Xie, S. Hong, and X. Chen, “Cell-selective metabolic labeling of biomolecules with bioorthogonal functionalities,” *Curr Opin Chem Biol*, vol. 17, no. 5, pp. 747–752, Oct. 2013, doi: 10.1016/j.cbpa.2013.07.006.

[57] M. Grammel and H. C. Hang, “Chemical reporters for biological discovery,” *Nat Chem Biol*, vol. 9, no. 8, pp. 475–484, Aug. 2013, doi: 10.1038/nchembio.1296.

[58] D. Zeng, B. M. Zeglis, J. S. Lewis, and C. J. Anderson, “The Growing Impact of Bioorthogonal Click Chemistry on the Development of Radiopharmaceuticals,” *Journal of Nuclear Medicine*, vol. 54, no. 6, pp. 829–832, Jun. 2013, doi: 10.2967/jnumed.112.115550.

[59] R. A. Evans, “The Rise of Azide–Alkyne 1,3-Dipolar ‘Click’ Cycloaddition and its Application to Polymer Science and Surface Modification,” *Aust J Chem*, vol. 60, no. 6, p. 384, 2007, doi: 10.1071/CH06457.

[60] L. Liang and D. Astruc, “The copper(I)-catalyzed alkyne-azide cycloaddition (CuAAC) ‘click’ reaction and its applications. An overview,” *Coord Chem Rev*, vol. 255, no. 23–24, pp. 2933–2945, Dec. 2011, doi: 10.1016/j.ccr.2011.06.028.

[61] L. Li, T. Pu, G. Zhanel, N. Zhao, W. Ens, and S. Liu, “New Biocide with Both *N* -Chloramine and Quaternary Ammonium Moieties Exerts Enhanced Bactericidal Activity,” *Adv Healthc Mater*, vol. 1, no. 5, pp. 609–620, Sep. 2012, doi: 10.1002/adhm.201200018.

[62] J. K. Kim, H. S. Cho, H. S. Jung, K. Lim, K. B. Kim, D. G. Choi, J. H. Jeong, and K. Y. Suh, “Effect of surface tension and coefficient of thermal expansion in 30 nm scale nanoimprinting with two flexible polymer molds,” *Nanotechnology*, vol. 23, no. 23, p. 235303, Jun. 2012, doi: 10.1088/0957-4484/23/23/235303.

[63] S. Y. Chou, P. R. Krauss, and P. J. Renstrom, “Nanoimprint lithography,” *Journal of Vacuum Science & Technology B: Microelectronics and Nanometer Structures Processing, Measurement, and Phenomena*, vol. 14, no. 6, pp. 4129–4133, Nov. 1996, doi: 10.1116/1.588605.

[64] G. Zhang, J. Zhang, G. Xie, Z. Liu, and H. Shao, “Cicada Wings: A Stamp from Nature for Nanoimprint Lithography,” *Small*, vol. 2, no. 12, pp. 1440–1443, Dec. 2006, doi: 10.1002/smll.200600255.

[65] X. Li, G. S. Cheung, G. S. Watson, J. A. Watson, S. Lin, L. Schwarzkopf, and D. W. Green “The nanotipped hairs of gecko skin and biotemplated replicas impair and/or kill pathogenic bacteria with high efficiency,” *Nanoscale*, vol. 8, no. 45, pp. 18860–18869, 2016, doi: 10.1039/C6NR05046H.

[66] D. Zhang, Y. Li, X. Han, X. Li, and H. Chen, “High-precision bio-replication of synthetic drag reduction shark skin,” *Chinese Science Bulletin*, vol. 56, no. 9, pp. 938–944, Mar. 2011, doi: 10.1007/s11434-010-4163-7.

[67] Z. Liu, Y. Yi, S. Wang, H. Dou, Y. Fan, L. Tian, J. Zhao, and L. Ren, “Bio-Inspired Self-Adaptive Nanocomposite Array: From Non-antibiotic Antibacterial Actions to Cell Proliferation,” *ACS Nano*, vol. 16, no. 10, pp. 16549–16562, Oct. 2022, doi: 10.1021/acsnano.2c05980.

[68] A. Bacchi, M. Costa, B. Gabriele, G. Pelizzi, and G. Salerno, “Efficient and General Synthesis of 5-(Alkoxycarbonyl)methylene-3-oxazolines by Palladium-Catalyzed Oxidative Carbonylation of Prop-2-ynylamides,” *J Org Chem*, vol. 67, no. 13, pp. 4450–4457, Jun. 2002, doi: 10.1021/jo0200217.

[69] L. Li, T. Pu, G. Zhanel, N. Zhao, W. Ens, and S. Liu, “New Biocide with Both *N* -Chloramine and Quaternary Ammonium Moieties Exerts Enhanced Bactericidal Activity,” *Adv Healthc Mater*, vol. 1, no. 5, pp. 609–620, Sep. 2012, doi: 10.1002/adhm.201200018.

[70] G. Reid, J. C. McCormack, O. Habimana, F. Bayer, C. Goromonzi, E. Casey, A. Cowley and K. M. Susan, “Biomimetic Polymer Surfaces by High Resolution Molding of the Wings of Different Cicadas,” *Materials*, vol. 14, no. 8, p. 1910, Apr. 2021, doi: 10.3390/ma14081910.

[71] B. Herigstad, M. Hamilton, and J. Heersink, “How to optimize the drop plate method for enumerating bacteria,” *J Microbiol Methods*, vol. 44, no. 2, pp. 121–129, Mar. 2001, doi: 10.1016/S0167-7012(00)00241-4.

[72] S.-H. Hong, J. Hwang, and H. Lee, “Replication of cicada wing’s nano-patterns by hot embossing and UV nanoimprinting,” *Nanotechnology*, vol. 20, no. 38, p. 385303, Sep. 2009, doi: 10.1088/0957-4484/20/38/385303.

[73] M. Sun, G. S. Watson, Y. Zheng, J. A. Watson, and A. Liang, “Wetting properties on nanostructured surfaces of cicada wings,” *Journal of Experimental Biology*, vol. 212, no. 19, pp. 3148–3155, Oct. 2009, doi: 10.1242/jeb.033373.

[74] J. Román-Kustas, J. B. Hoffman, J. H. Reed, A. E. Gonsalves, J. Oh, L. Li, S. Hong, K. D. Jo, C. E. Dana and D. M. Cropek, “Molecular and Topographical Organization: Influence on Cicada Wing

Wettability and Bactericidal Properties," *Adv Mater Interfaces*, vol. 7, no. 10, May 2020, doi: 10.1002/admi.202000112.

[75] L. Duta, A. C. Popescu, I. Zgura, N. Preda, and I. N. Mihailescu, "Wettability of Nanostructured Surfaces," in *Wetting and Wettability*, InTech, 2015. doi: 10.5772/60808.

[76] T. Ren, T. V. Dormitorio, M. Qiao, T.-S. Huang, and J. Weese, "N-halamine incorporated antimicrobial nonwoven fabrics for use against avian influenza virus," *Vet Microbiol*, vol. 218, pp. 78–83, May 2018, doi: 10.1016/j.vetmic.2018.03.032.

[77] B. Demir, R. Broughton, M. Qiao, T.-S. Huang, and S. Worley, "N-Halamine Biocidal Materials with Superior Antimicrobial Efficacies for Wound Dressings," *Molecules*, vol. 22, no. 10, p. 1582, Sep. 2017, doi: 10.3390/molecules22101582.

[78] Z. Cao and Y. Sun, "Polymeric *N* -Halamine Latex Emulsions for Use in Antimicrobial Paints," *ACS Appl Mater Interfaces*, vol. 1, no. 2, pp. 494–504, Feb. 2009, doi: 10.1021/am800157a.